

COMPARISON OF 3D OPPOSED JETS GEOMETRIES: 3D COMPUTATIONAL FLUID DYNAMICS (CFD) STUDY

Ertuğrul ERKOÇ *

¹ Department of Chemical Engineering, Engineering and Architecture Faculty, Bursa Technical University, Bursa

ABSTRACT

Influence of geometry on the mixing mechanism and efficiency is studied by comparing Opposed Jets of Cylindrical and Prismatic shapes, having the same hydraulic chamber diameter by 3D Computational Fluid Dynamics (CFD) models. For the test case, same Reynolds numbers of the jets were provided. The comparison is assessed by hydrodynamics, turbulence parameters and mass transfer inside the mixing chambers. While the hydraulic diameters of the chambers set as equals, the thickness of the jets of the T-Jets mixers set as the diameters of the jets of the Confined Impinging Jets, which resulted in non-equal hydraulic diameters of the Jets. The power spectra of the x and y velocities for T-Jets showed a similar peaks as in 2D chambers, however without the spread of the energy. The results suggests that for T-Jets, Reynolds numbers of the jets alone is not enough to describe the mixing inside the chamber, but the thickness of the jets is also an important parameter since different values of jets thicknesses and depths can provide the same hydraulic diameter. Finally, this study shows that on one hand CIJ promotes a more intense striation of the initial flow scales when compared to the T-jets, on the other hand the latter promotes a broader impingement region and allows larger inlet areas, i.e. higher throughputs, for the same initial scale. The choice of the mixer should then be the trade-off between these two factors. For a better comparison, the same hydraulic diameters of the jets giving the same Reynolds numbers should be investigated.

Keywords: T-Jets, Confined impinging jets, CFD, Mixing, Opposed jets

1. INTRODUCTION

Opposed jet mixers are particularly suited for fast chemical reactions, such as reactive polymerizations [1] or fast precipitations [2, 3]. These mixers can be either cylindrical or prismatic. The cylindrical geometries have two round jets and are generally called Confined Impinging Jets (CIJ), while the prismatic geometries have slot jets that extend over the whole depth of the channel and are generally called T-jets mixers. Although having the same principle of mixing, i.e., two opposed jets impinging each other, the geometries they have may provide different mixing mechanisms and efficiencies.

Geometry influence on mixing in opposed jet reactors has been seldom studied, particularly the focus of this study: the comparison of cylindrical and prismatic opposed jet mixers and the relation of the flow field on such geometries with 2D results from CFD simulations [4]. A recent work of [5] focused on the comparison of Y and T mixers (prismatic geometries) with Opposed Impinging Jets mixers (cylindrical geometry) using as micromixing test reactions a fast acid-base neutralization (HCl+NaOH) and as second slower reaction acid-catalyzed hydrolysis of 2,2-dimethoxypropane (C) to acetone and methanol. Nevertheless, a work on the comparison of the flow on CIJ and T-jets is not available from the literature, so far there are only works focusing separately in each geometry type.

Previous studies on CIJ or T-jets geometries are mostly concerned on either the effect of injectors to chamber diameter ratio, configuration of the injectors connected to the mixing chamber mainly on the connection angle, and outlet designs [6-8]. The studies concerning the injectors to chamber diameters ratio effect on the hydrodynamics show that the effect of important operational parameters, such as the Reynolds number, depends on the injectors to chamber diameter/width ratio [9]. The studies of [9]

*Corresponding Author: ertugrul.erkoc@btu.edu.tr

show that increasing the ratio of the injectors to chamber diameter increases the critical Reynolds number necessary for chaotic mixing inside the chamber. On the other hand some early studies [10, 11] suggested that injectors to chamber ratio had no significant effect on flow field, although the majority of those studies [3, 6, 12-15] stated that increasing the ratio makes the mixing poorer for a given operational Reynolds number. Studies of Sebastian and Boukobbal [16] suggested that increasing the ratio of the nozzle diameter to the chamber diameter improved the mixing and suggested a nozzle diameter equal to the mixhead diameter while leaving the other nozzle with an adjustable diameter to satisfy momentum balancing would be desirable. Jie and his coworkers [17] stated that increasing the ratio of nozzle to chamber diameter increases the turbulent intensity inside the chamber. However, all of these studies were performed using cylindrical injectors having circular cross-sections and hence increasing the jets diameter meant making the cross-section bigger in all space dimensions.

Denschikov and his coworkers [13] observed that for self-sustained oscillations to take place, the diameter of the chamber should be bigger than 2-3 times the transverse dimensions of the jets. This is explained from CFD results of [9] that highlighted as the most probable mechanisms underlying this flow stabilization the fact that increasing the injectors diameter / width ratio thickens the feed streams which results in less free space between the jets and mixing chamber walls for the formation of fully developed vortices.

Although the mentioned researchers studied the design effect of the chamber, they mainly studied the design parameter of a particular geometry: injectors to chamber diameter ratio, outlet configuration, and the angle formed by the axes of the injectors and the axis of the mixing chamber. There are no studies, which the authors of this article is aware of, investigating the effect of geometrical shape of the reactor: cylindrical (CIJ), prismatic (T-jets) or 2D. This article presents a comparative 3D computational study of a prismatic chamber having the rectangular injectors that extend throughout the all chamber depth, and a cylindrical chamber with cylindrical injectors. The results from both geometries are compared with the results from the 2D model, this comparison gives further insight into the analysis of the results for the 2D model and their application to actual 3D geometries.

2. 3D CFD MODEL

Views of RIM mixing chambers having a CIJ or T-jets geometry are shown in Figure 1. The cylindrical chamber with chamber diameter of 10 mm has two injectors of 1.5 mm diameters.

The T-jets chamber is rectangular and has the same width (x -direction in Figure 1) and depth (z -direction in Figure 1) – 10mm, i.e. the chamber cross section is square and has the same hydraulic chamber diameter with the cylindrical one. The axis of the opposed injectors in the T-jets and also in the CIJ chambers are at 5mm from the closed top of those chambers. For both geometries the flow enters to the mixing chambers symmetrically via the injectors with the same Reynolds number, and exits the mixers at the open side of the chamber - the outlet. The main differences are the cross sections of the chambers and the injectors. The cross section of the chamber is a circle for the case of CIJ and a square for the T-jets. The injectors in the CIJ are circular with a diameter of 1.5mm while in the T-jets chamber the injectors extend throughout all the depth of the mixing chamber, i.e. the width of the injectors is 10mm, and the height of the injectors is 1.5mm.

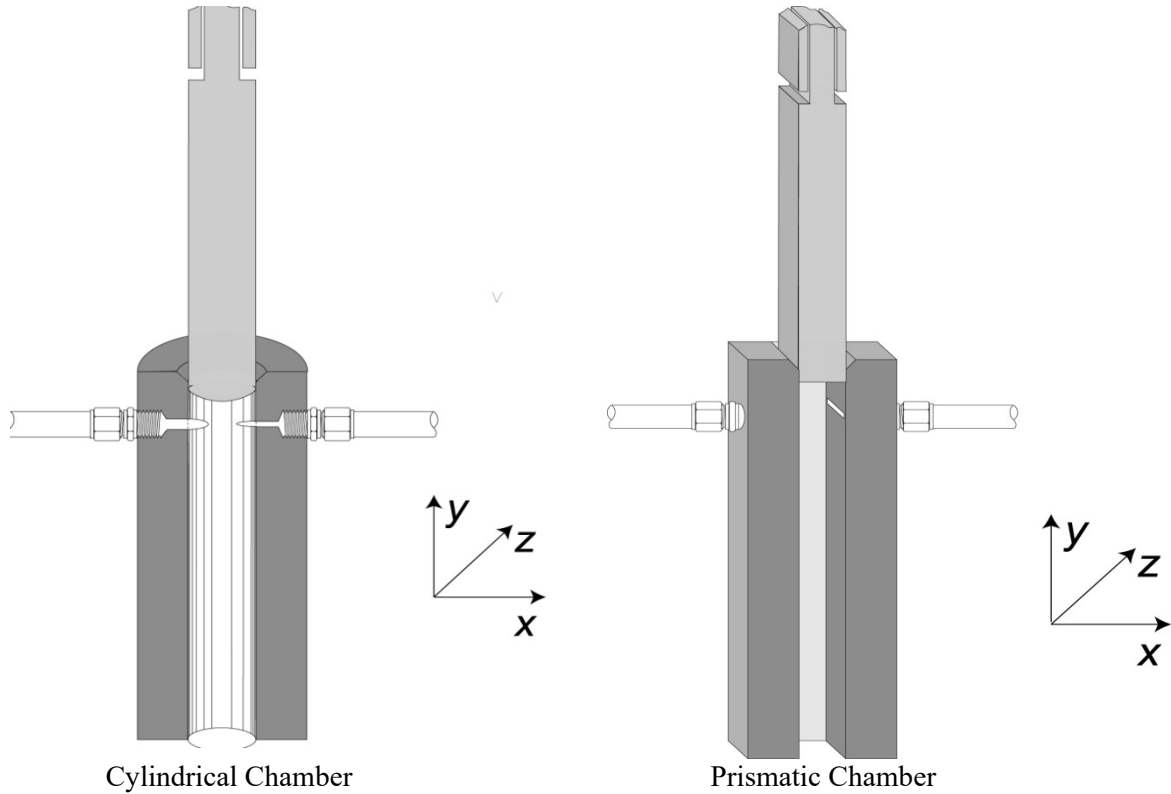


Figure1. Schematic view of the cylindrical and prismatic chambers

The CFD simulations of the opposed jets mixers were performed using a grid and time step interval smaller than all the space and time scales of the flow field: Direct Numeric Simulation (DNS). The equations solved are the continuity or mass conservation equation for incompressible flows,

$$\nabla \cdot \vec{v} = 0 \quad (1)$$

where \vec{v} is the velocity vector, and the Navier-Stokes equations,

$$\rho \frac{D\vec{v}}{Dt} = -\vec{\nabla} p + \mu \nabla^2 \vec{v} + \rho \vec{g} \quad (2)$$

where p is the static pressure and \vec{g} the gravity acceleration vector. The 3D simulations were performed using the commercial CFD code FluentTM in a computational cluster IBM eServe 1350 with 32 nodes and 64 CPUs. The geometries used in CFD simulations are shown in Figure 2 for cylindrical chamber (CIJ) and in Figure 3 for the prismatic chamber (T-Jets). The planes where data was extracted for the flow maps are shown in Figure 4. The same Reynolds number of the jets and working fluid were used on both simulations, the Reynolds number was 300 and the fluid had a viscosity $\mu = 0.020 \text{ Pa} \cdot \text{s}$ and density $\rho = 1200 \text{ kg/m}^3$. Although the geometries of the chambers and of the injectors are different from each other, the hydraulic diameter of the jets differs between the CIJ and the T-jets, thus the velocity of the jets entering the mixing chamber are different. With the given geometrical parameters for the prismatic chamber, the hydraulic diameter of the injectors, $D_{H, inj}$ is calculated according to

$$D_{H, inj} = \frac{4A_{inj}}{U_{inj}} \quad (3)$$

where A_{inj} is the cross sectional area of the injector and U_{inj} is the wetted perimeter of the cross section. The Reynolds number is defined at the injectors as,

$$Re = \frac{D_{H,inj} v_{inj} \rho}{\mu} \quad (4)$$

where v_{inj} is the superficial velocity at the injectors. For both geometries, the operational Reynolds number was set at 300.

2.1. Boundary and Initial Conditions

No slip boundary condition was assumed for the walls of both chambers, i.e., the three velocity components tangential at the mixing chamber walls were set to zero. Let us now consider this boundary condition continuity at a position of the chamber wall aligned with the y and z axes, thus $v_y = v_z = 0$ in the neighborhood of this position and as a consequence

$$\frac{\partial v_y}{\partial y} = \frac{\partial v_z}{\partial z} = 0 \quad (5)$$

and from the continuity equation

$$\nabla \cdot \mathbf{v} = 0 \Rightarrow \frac{\partial v_y}{\partial y} + \frac{\partial v_z}{\partial z} = -\frac{\partial v_x}{\partial x} = 0 \quad (6)$$

then, at the walls both the velocity components and their derivatives are zero.

At the inlet of the injectors, the x velocity component is set to the values of the superficial velocity at the injectors, $v_x = v_{inj}$, while the other velocity components are set to zero. Using the same reasoning as above it comes that the space derivatives of the velocity components at the mixing chamber inlet are also zero.

At the exit of the chambers pressure outlet conditions were set. These boundary conditions set a constant value for the static pressure at the outlet, in the present case the outlet pressure was assumed equal to the atmospheric pressure.

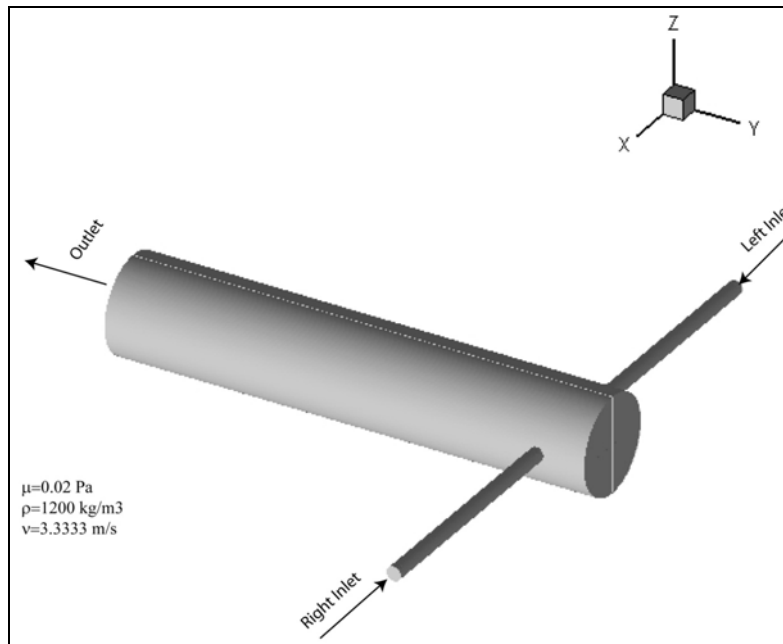


Figure 2. Geometry and operational parameters of the cylindrical chamber used in CFD simulation

The CFD simulations were initially performed for a steady state simulation and the dynamic simulations started from the obtained steady state simulations. The computational grid for the cylindrical chamber consisted of 1.8×10^5 cells, and the grid for the prismatic chamber consisted of 8.5×10^5 cells. The simulations were performed using 2nd order implicit pressure based solver using velocity-pressure coupling SIMPLEC method with 2nd order pressure and 3rd order momentum discretization. The simulations were performed for 2 seconds of operation with time step of 10^{-4} seconds. The velocity components at the probed points were recorded every time step, i.e., every 10^{-4} seconds of operation. The probed points were distributed throughout the mixing chamber axis at distances from the top of the chamber $y=5, 11, 22, 33,$ and 44 mm. The point at $y=5$ mm corresponds to the impingement point of the jets. For every 10 time steps, i.e. each 1 ms, the complete files with the complete solution from the CFD simulations were saved, which makes the dynamic presentations of frames of velocity maps possible. In this article, only snapshots of selected time steps are going to be shown.

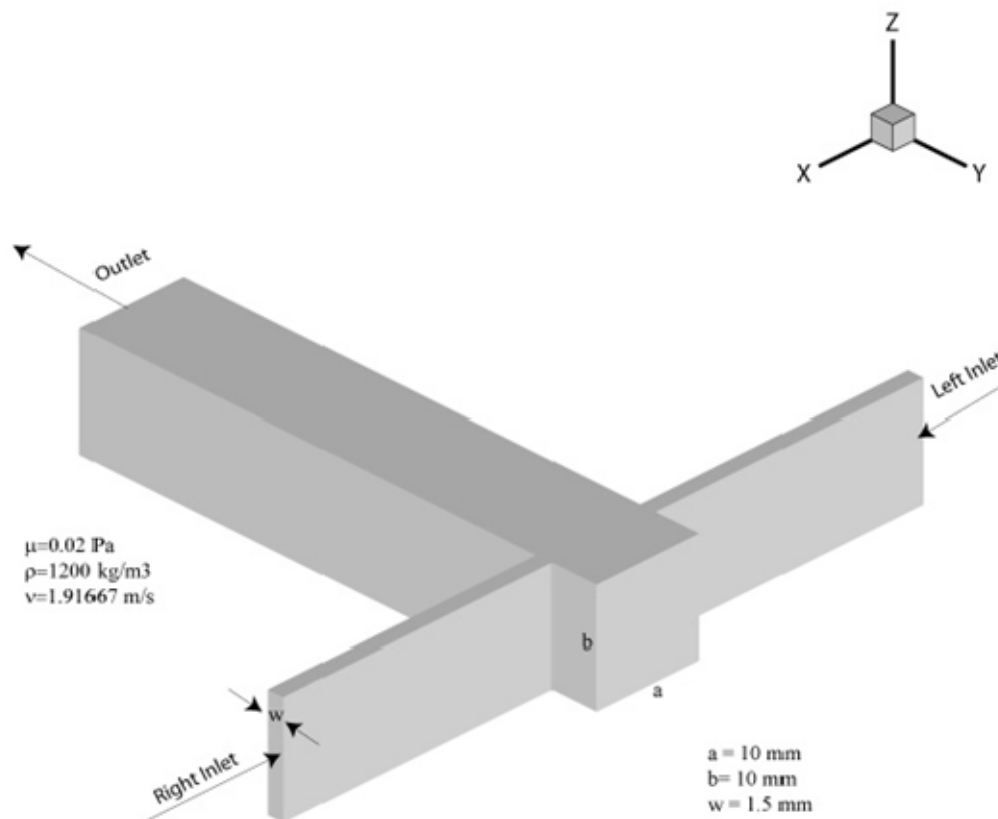


Figure 3. Geometry and operational parameters of the prismatic chamber used in CFD simulation

For both geometries simulations, the residues of the solution vector, i.e. the maximum deviation the solved equations could have from the equalities in Equations 1 and 2 was.

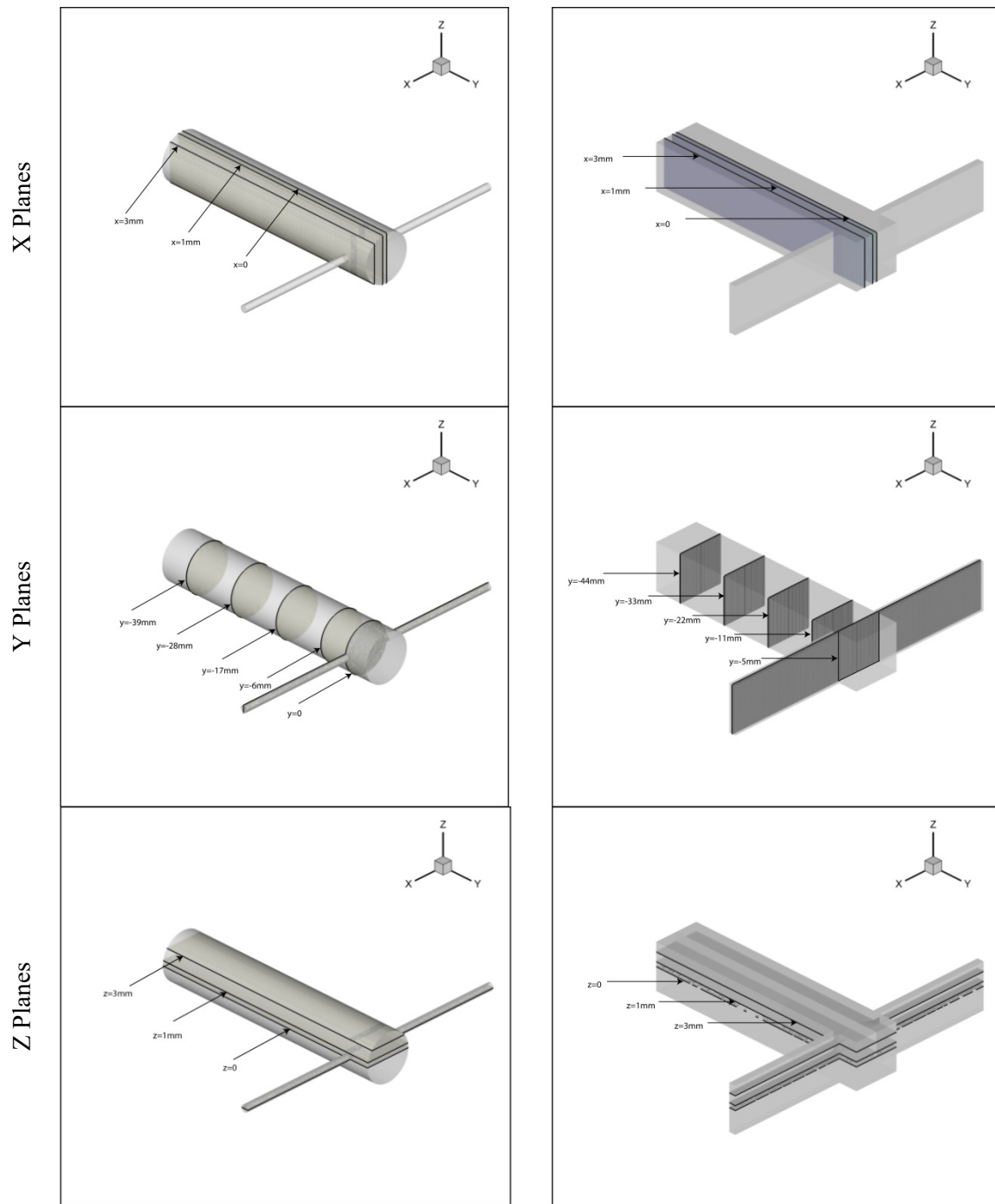


Figure 4. Representation of the planes for the two chambers

2.2. Spectral Analysis

The power energy spectra of the U_x , U_y and U_z velocity components were computed at the probed points in the chamber axis. The power energy spectrum were computed from the Discrete Fourier Transform, DFT, of the time series of the velocity components for 1 second of operation for T-jets / prismatic chamber, and 1.7 seconds of operation for the CIJ chamber. The DFT is defined as:

$$G\left(\phi = \frac{k}{N\Delta t}\right) = \sum_{i=1}^{N-1} v_x(i\Delta t) e^{-j2\pi ik/N}, \quad k = 0, 1, 2, \dots, N \quad (7)$$

where $v_x(i\Delta t)$ is the velocity time series, Δt is the interval of the time series, ϕ is the frequency, N is the total number of points in the time series and $e^{-j2\pi ik/N}$ is the Euler form for a complex number where j is the imaginary part.

The first second of operation for the T-jets was omitted while for the CIJ only the first 300ms of operation were omitted. In both cases the initial part of dynamics data that was removed was the transient period where the flow evolved from a steady state to a self-sustainable chaotic flow, this way the data for the power spectra only considers the chaotic flow regime.

3. COMPARATIVE STUDY OF HYDRODYNAMICS

3.1. Steady State Solutions

The dynamics of the convective flow patterns were proven to be the main mixing mechanism in opposed jets mixers by [18]. So, from the steady state solutions one cannot assess the dynamics and the degree of mixing inside the opposed jets mixing chambers. Nevertheless, the steady state solutions show the overall flow patterns and the location and shape of the vortices that will be dynamically evolving at higher Reynolds numbers.

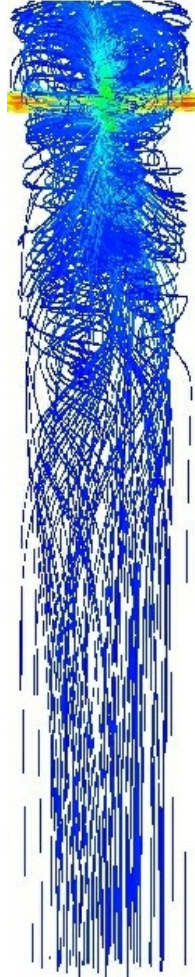
Imaging 3D flow fields on paper is a complex task ([19] and [20]), because of this here are presented both pathlines and velocity vector maps of the flow field at the several planes shown in Figure 4.

Figure 5 shows the pathlines formed from the injectors up to the outlet both for the OJR and the T-jets. Figure 6 shows a zoom of the pathlines close to the jets impingement region. These pathlines were obtained using Tecplot®, which computes the pathline of a particle released from specified points. In the present case the particles were only tracked in specific time instants of a dynamic flow field, which corresponds to the actual flow field in the case of steady state flow regimes. In both geometries the opposite jets impinge inside the mixing chamber at an equidistant location from the opposite injectors generating a symmetric flow field. The jets in the CIJ follow a straight line from the injectors until the impingement point. After impinging each other the fluid from the jets spread radially forming a pancake like structure [21]. The jets in the T-jets extend throughout the whole depth cutting any paths for convective transport of mass from the upper part of the mixing chamber. Because of this the jets are forced to bend towards the outlet and the impingement line is below the injectors axis. After impinging each other the jets flow parallel to the outlet through the central region of the mixing chamber.

On both chambers the jets are surrounded by vortices, although these vortices are quite different in the CIJ and in the T-jets. In the OJR two vortices are formed, one around each jet. From the pathlines in Figure 5 and Figure 6 the rotation of the flow around the jets is clear. The vortex rotates in front of and in the back of the jet with a rotation axis in the y axis direction. The vortex is united over the jets where its rotation axis is on the z direction. The vortices in front of and in the back of the jets are clear from the vector maps of the y -planes $y=-5\text{mm}$ and $y=-11\text{mm}$ in Figure 7. The rotation of fluid over the jets is clear from the vector maps extracted at the z -planes, see

Figure . The rotation axis of the vortices formed in the OJR is an arc passing over the jet and then bending downstream up to $y = -11\text{mm}$. For regions further downstream, see $y = -22\text{mm}$ in Figure 7, these vortices are not clear.

Path lines for Cylindrical Chamber



Path lines for Prismatic Chamber

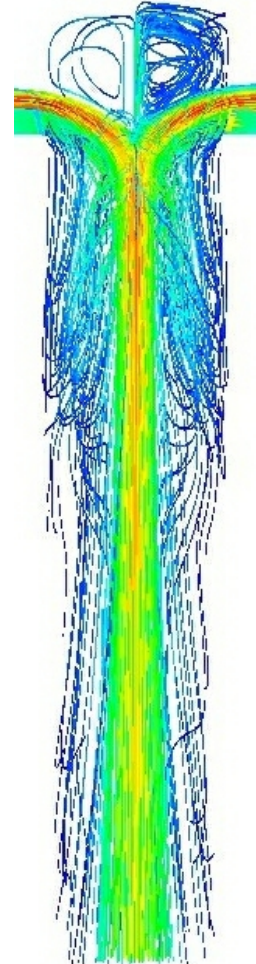


Figure 5. Pathlines along the chambers

Pathlines in Cylindrical Chamber

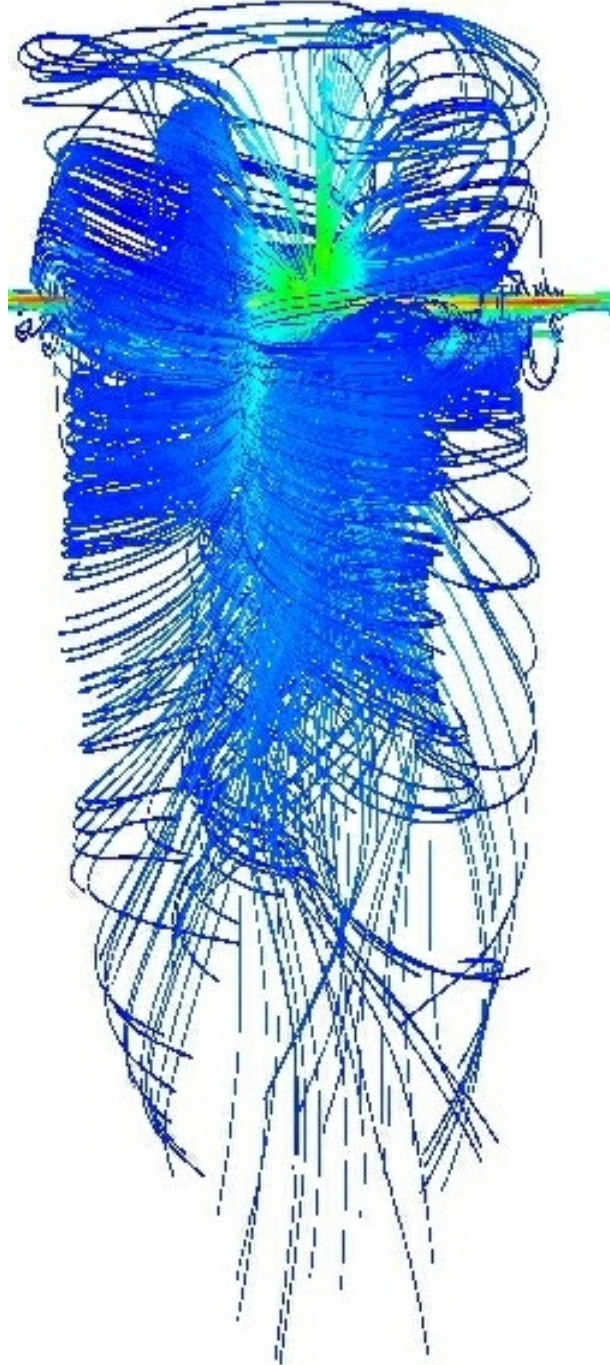


Figure 6. Detailed view of the pathlines for the cylindrical chambers in the impingement region

The prismatic chamber has four vortices: one vortex above each jet forming a pair of vortices above the jets; and one vortex below each jet forming another pair of vortices below the jets. The pair of vortices above the jets is clear both from the pathlines in Figure 5 and Figure 6 and also from the vector maps in the z-planes, see Figure 8. These vortices are approximately rounded due to the aspect ratio of the top of the chamber which has a height (5mm) equal to half the chamber width (10mm). Below the jets the vortices are elongate in the direction of the chamber outlet, this is particularly clear from the pathlines in Figure 5.

In the prismatic chamber the mass transfer between the upper vortices and the bottom vortices is reduced, which is clear from the vector maps in Figure 8 that show the jets path. The jets feed the rotation of the upper and bottom vortices although due to the fact that the jets extend throughout the chamber depth they segregate the right and left side vortices and the top and bottom vortices.

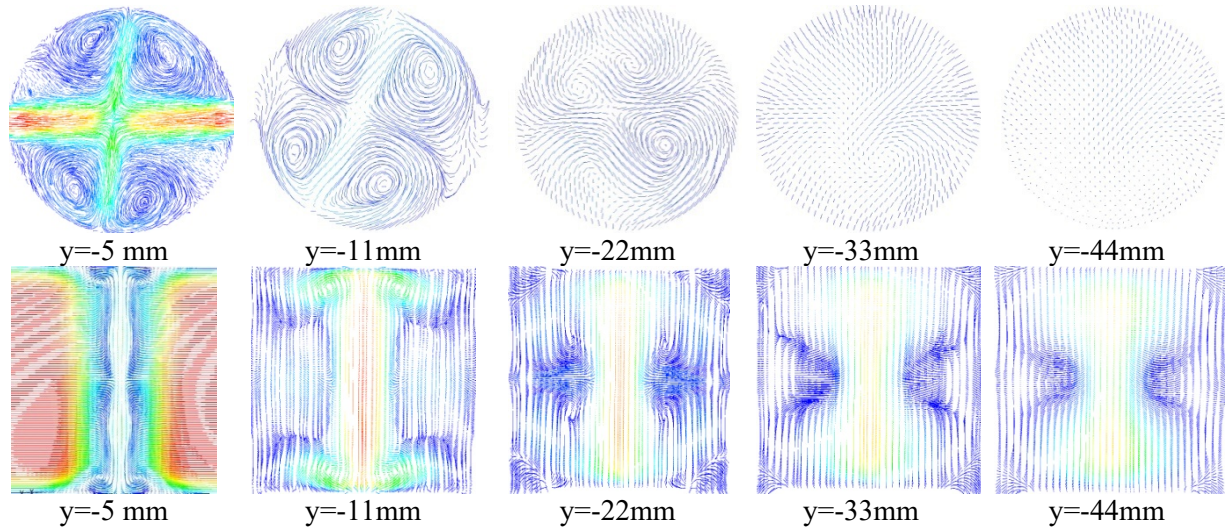


Figure 7. Vector maps in y planes for the cylindrical and prismatic mixing chambers

Figure 9 and Figure 10 show the pathlines in the cylindrical and prismatic chambers originated:

1. from a cross centered at the injectors axis for the cylindrical chamber;
2. from a single line at the center of only one of the injectors for the prismatic chamber.

These two figures were published in [4] and clearly highlight the features described above for the cylindrical and the prismatic chambers. For the cylindrical chamber the shape of the vortex is very clearly observed. The vortex rotates around the jet and dissipates downstream the jets impingement point at a distance approximately equal to the mixing chamber diameter. From Figure 9 are particularly clear the rotation axis of the vortices in the y direction at positions downstream the jets and the arc formed by the vortex rotation axis over the jet.

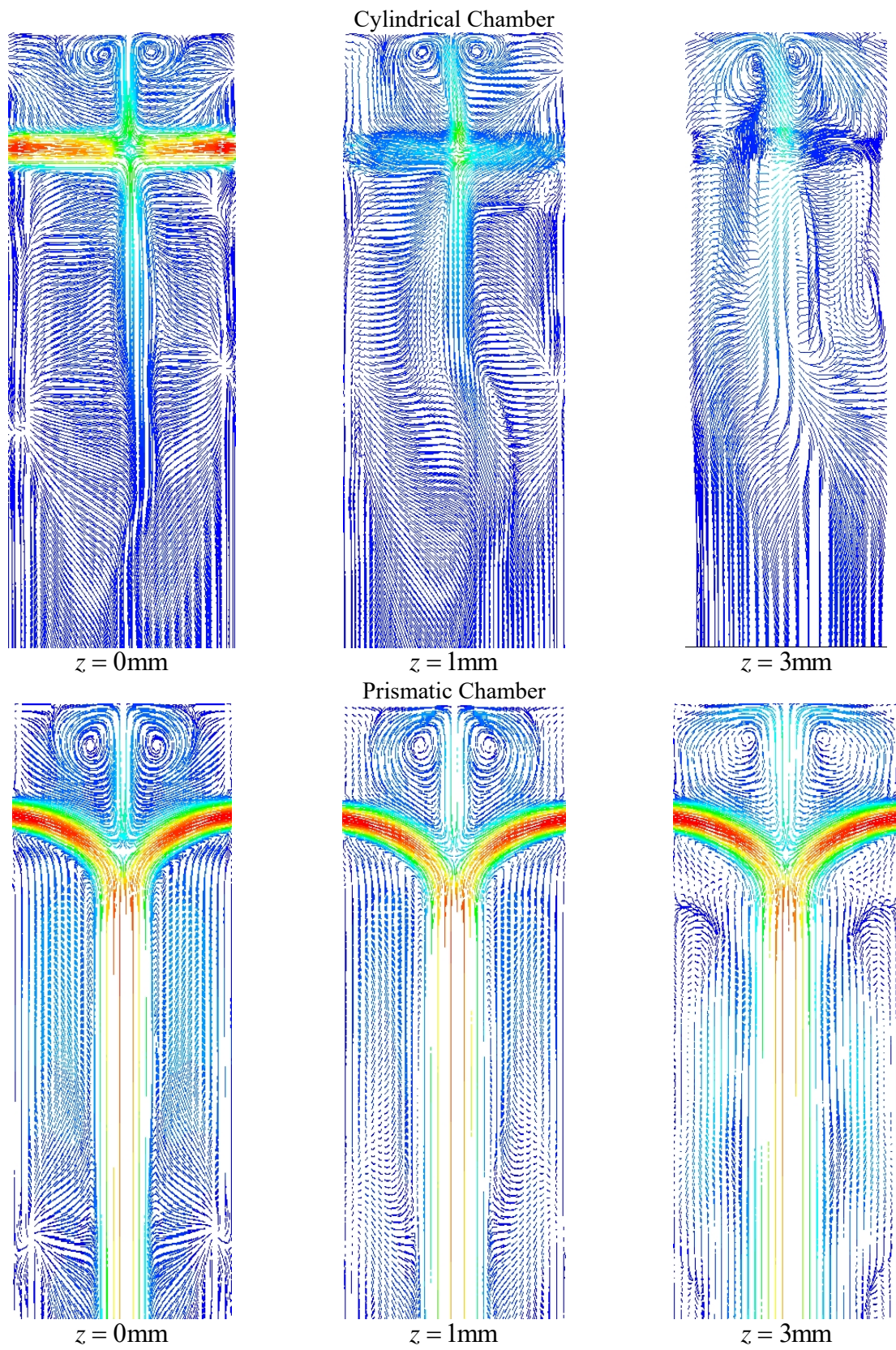


Figure 8. Vector maps in z planes for the cylindrical and prismatic mixing chambers

The flow patterns in the prismatic chamber are also particularly clear from the pathlines in half of the mixing chamber shown in Figure 10. The two features that are more noticeably observed are:

1. The path formed by the jets while going from the inlet to the outlet through the mixing chamber center. The jets keep their inlet speed and as seen from Figure 5 and Figure 8 they flow side by side from the impingement point to the outlet. The jets width is also kept throughout the chamber.
2. The way the upper vortices are segregated from the rest of the chamber by the jets is particularly clear in Figure 10. From the jets only a small fraction of flow goes to the upper vortices, the pathlines show that this small fraction of the fluid gets stuck in the upper vortex spinning several times before escaping through the region close to the chamber wall.

The jets width is the length that must be overcome by diffusion for mixing to occur at steady flow regimes. In prismatic chambers the jets width is kept roughly the same from the injector until the chamber outlet. In cylindrical chambers there is a strong initial striation of the jets, which spread radially after impinging each other, and in this way the distance for diffusion to occur is reduced by a factor around ten. The striation of the jets in the cylindrical chamber is clear in the Planar Laser Induced Fluorescence (PLIF) images shown in Figure 11. The PLIF images were obtained in a plane of the mixing chamber, plane $z = 0\text{mm}$, and show the concentration maps in that plane when a jet dyed with Rhodamine impinges a clear jet. From the image in Figure 11 it is clear the initial scale of the jet equal to the injector diameter and the tenfold reduction of this scale after the jets impingement point.

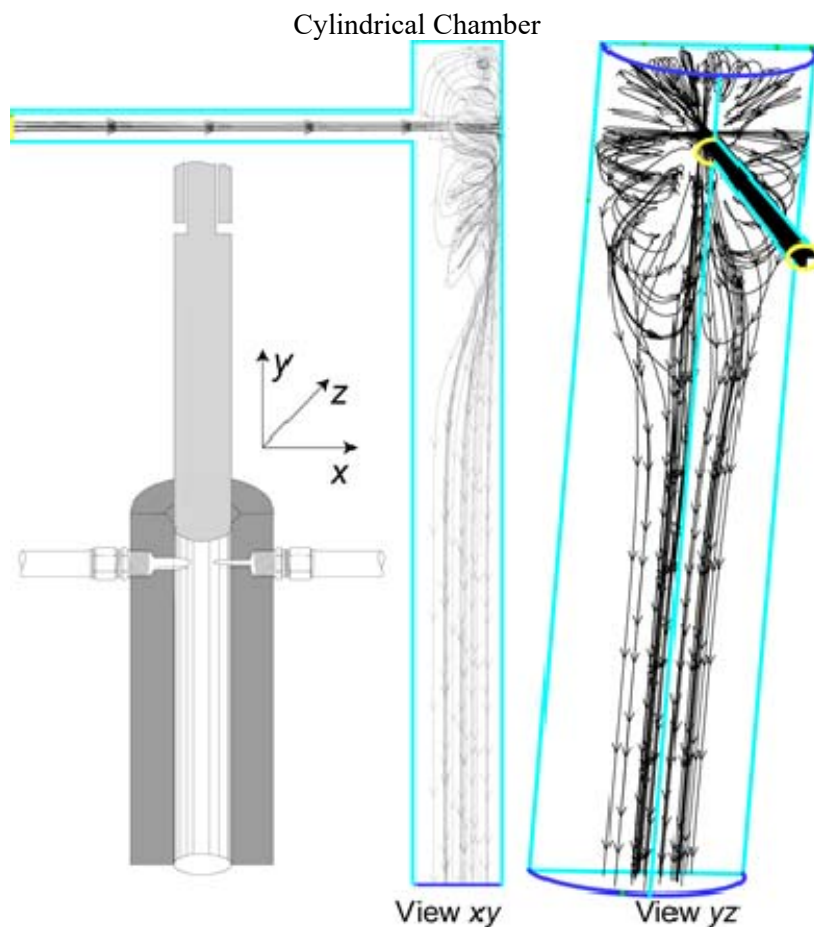


Figure 9. Pathlines released from a single line at the center of the injectors in the cylindrical chamber

Prismatic Chamber

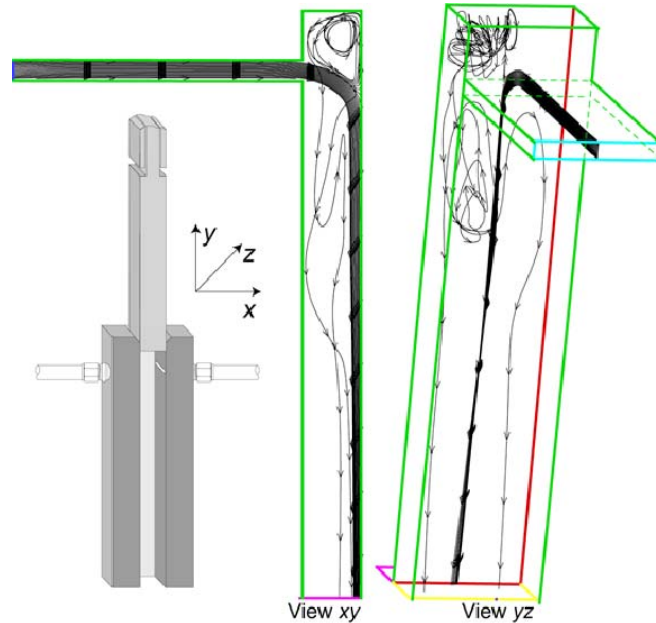


Figure 10. Pathlines released from a single line at the center of the injectors in the prismatic chamber

This study shows that on one hand CIJ promotes more intense striation of the initial flow scales when compared to the T-jets, on the other hand the latter promotes a broader impingement region and allows larger inlet areas, i.e. higher throughputs, for the same initial scale. The choice of the mixer should then be the trade-off between these two factors. The observations made in this section are restricted to CIJ and T-jet mixers operating in steady state flow regimes. Nevertheless, due to the choice of operational conditions and design many opposed jet mixers, particularly micromixers, operate at steady state segregated flow regimes, see [22], [23] and [24]. The next section is going to analyze the differences between flow fields in OJR and T-jets at dynamic flow regimes.

Cylindrical Chamber

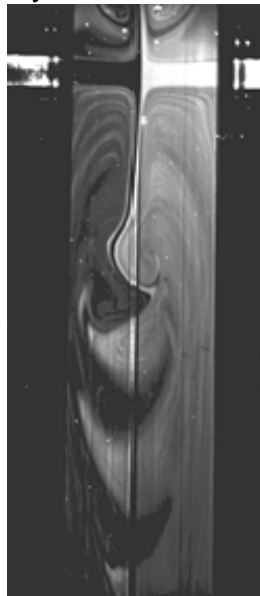


Figure 11. PLIF image of the cylindrical chamber for $Re = 100$

3.2. Dynamic Simulations

The dynamic evolution of the flow was simulated by means of CFD simulation. The simulations were direct numerical simulations (DNS) where all the time and space scales of the flow are larger than the discretization time interval and numerical grid, respectively ([25]). The DNS, also called numerical experiments, will enable obtaining the vector maps of the flow field, time histories of the velocity components at some points and respective spectral analysis of these time histories. These data will be used to draw the dynamic features of the 3D flow fields. In the following section will also be shown CFD results using turbulence models to compare the energy dissipation distributions in the different geometries.

3.2.1. Flow field

Figure 12 shows the vector maps on the $z = 0$ plane, and Figure 13 on the $y = 0$ from the CFD dynamic simulations at three distinct time instants for $Re = 300$. The maps in these figures show distinct flow patterns at the different time instants, thus the flow inside the chamber is dynamic; however, considering the low Reynolds number, $Re = 300$, and the absence of smaller scale vortices, the flow is not turbulent. One dynamic feature of this flow field that can be extracted from the vector maps in Figure 12 and Figure 13 is that the impingement point position is evolving.

In the prismatic chamber, after impinging each other, the jets are directed towards the outlet, whereas in the case of the cylindrical chamber the jets spread radially forming a pancake like structure. The jets paths after the impingement point evolve dynamically at $Re = 300$. As a consequence the vortices that are located around each jet become distorted and the symmetry of the flow fields in both chambers is completely broken. The elongated symmetrical vortices placed downstream in the mixing chamber, see the steady state simulations vector maps in Figure 8, at the dynamic flow regime become roundish and are no longer symmetrical.

In the prismatic chamber is observed from Figure 12 that both jets bend towards the outlet before impinging each other. The two opposed jets merge in a single jet issuing from the impingement point. The merged jet is directed towards the outlet and is alternately bend to the left and the right side of the mixing chamber axis by action of the side vortices that engulf this jet with the surrounding fluid. Because of this, the merged jet does not flow until the outlet of the mixing chamber as it did in the steady flow regimes. Nevertheless, in the prismatic chamber the jets are directed towards the outlet roughly keeping the speed of the inlet jets as can be seen from the vector maps in Figure 7. The fact that the jets are directed towards the outlet without decelerating, rather than being spread radially as in cylindrical chamber, promotes a stronger dynamics of the flow up to further downstream positions in the prismatic mixing chamber. The effects of the flow patterns on the flow dynamics will be clear in the following paragraphs from the analysis of the local time histories of the velocity components.

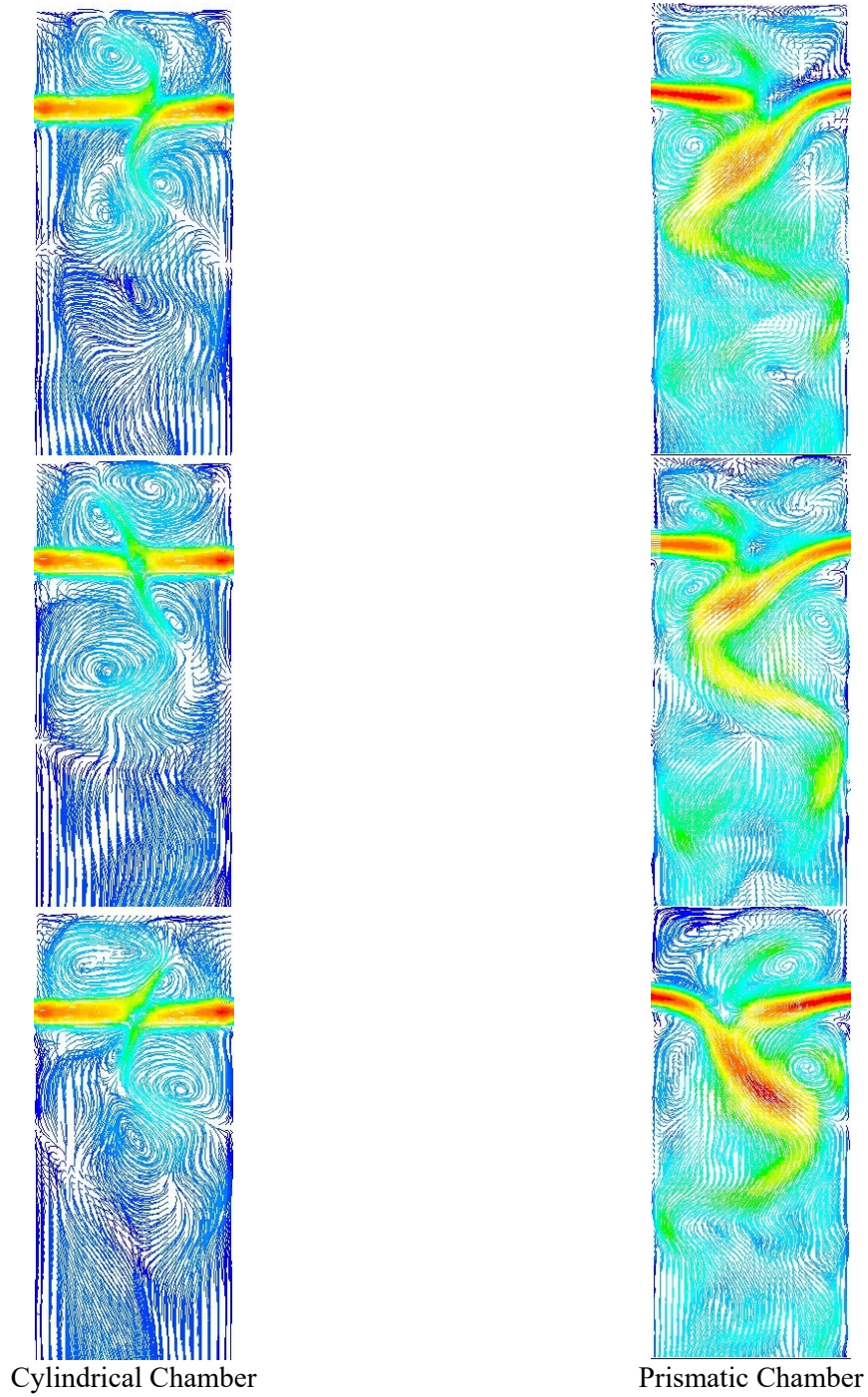


Figure 12. Vector maps on $z=0$ plane for three different time instants

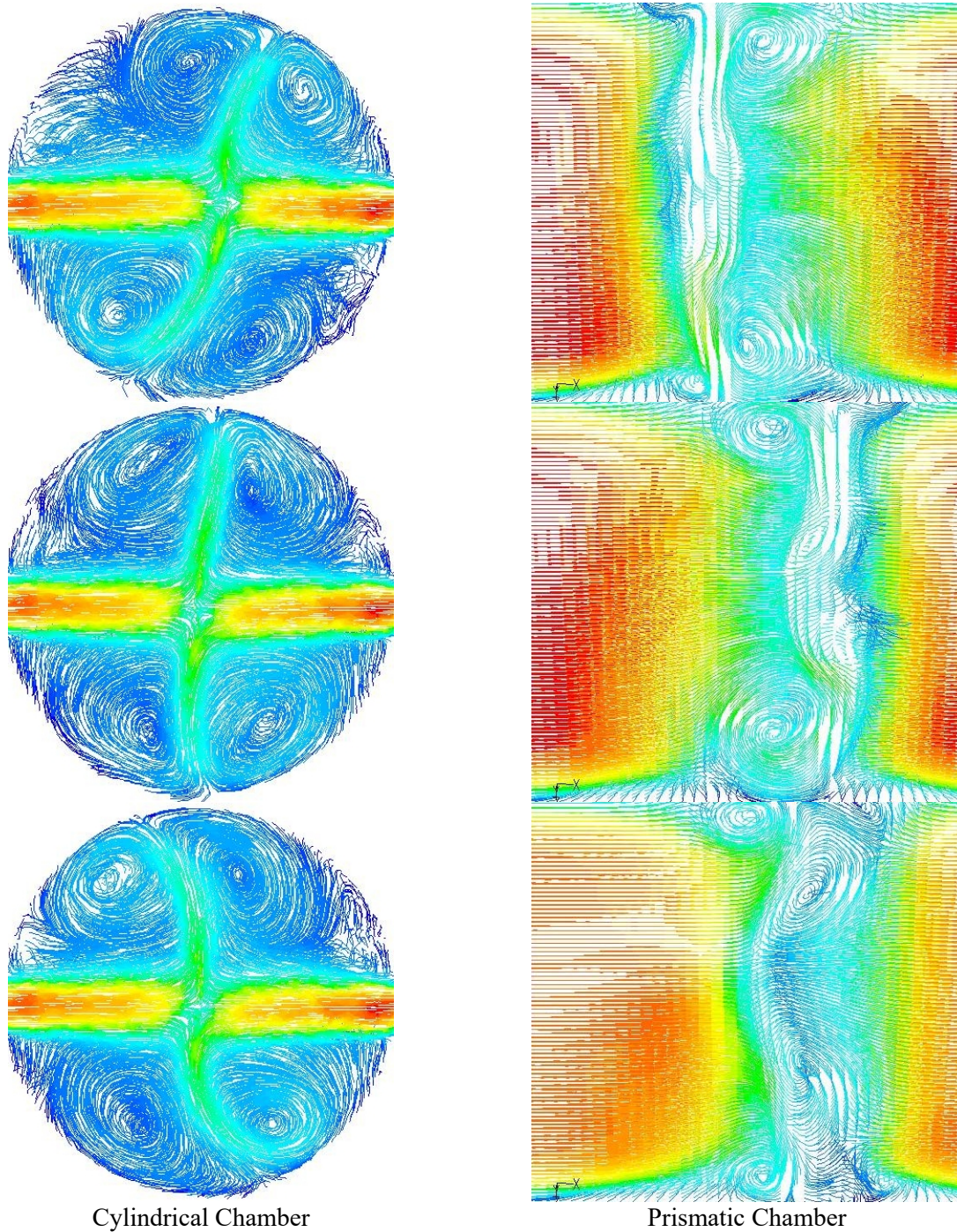


Figure 13. Vector maps on $y=0$ plane for three different time instants

A more detailed view of the dynamic flow field in the cylindrical mixing chamber is shown in Figure 14, which was originally published in [26] using a Cartesian coordinate system with a different orientation than the one used in the other figures of this chapter. In this figure are shown vector maps at several planes of an instantaneous flow field at $Re = 300$. Figure 14 shows more clearly the flow patterns in the cylindrical mixing chamber at dynamic flow regimes: namely, the radial spreading of the jets and the shape of the vortices that engulf those jets.

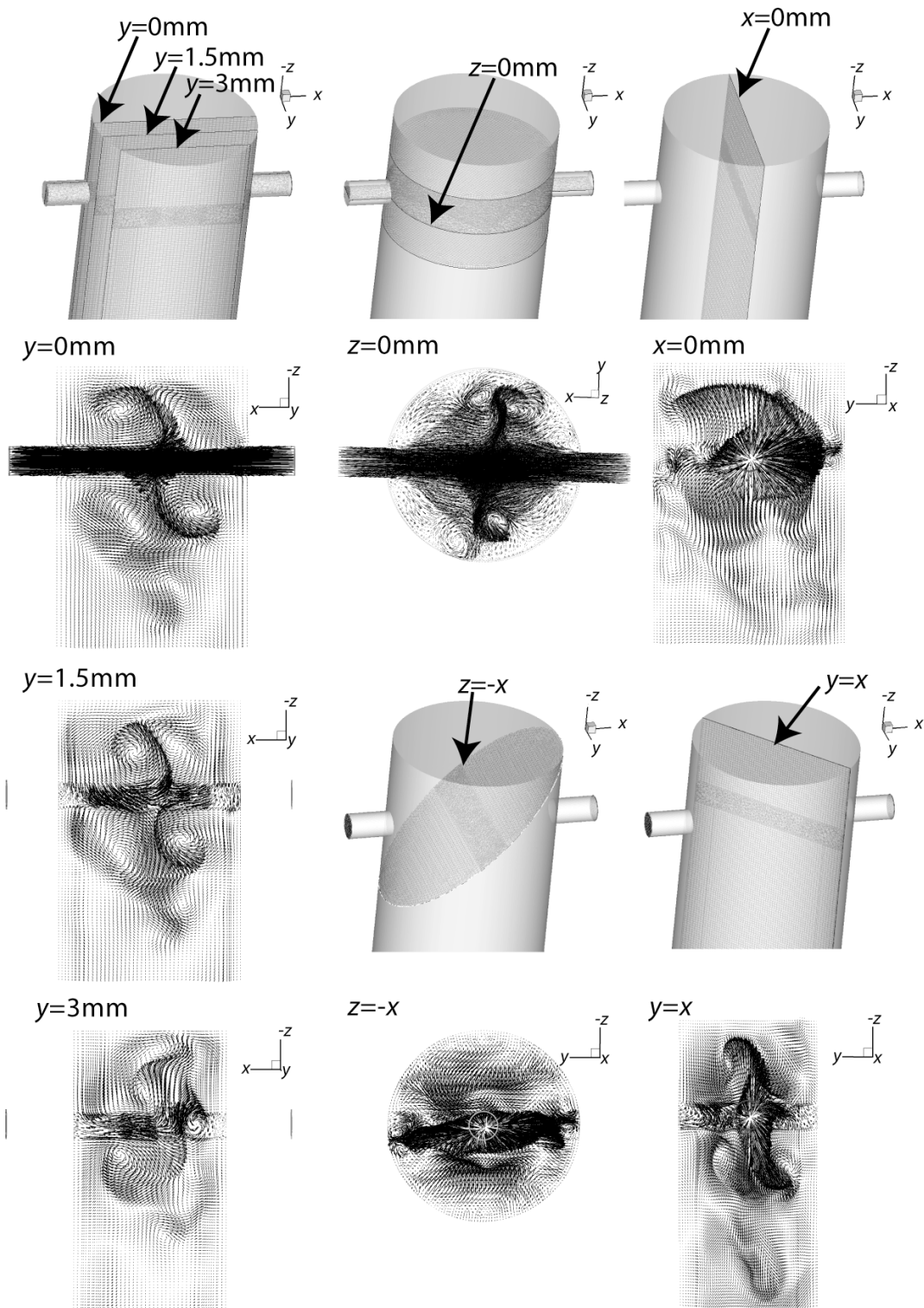


Figure 14. Vector maps in the cylindrical mixing chamber at $Re=300$ [26]

3.2.2. Flow dynamics

Figure 15, Figure 16, and Figure 17 show the time histories of U_x , U_y and U_z , respectively, at five points located in the mixing chambers axis at distances from the mixing chambers top of 5, 11, 22, 33

and 44 mm ($y = -5, -11, -22, -33$ and -44 mm). The time histories of the three velocity components fluctuate around an average value, which is approximately zero for the case of the velocity components that are normal to the chamber axis: x and z . Although the instantaneous flow fields in dynamic regimes are asymmetrical, the average flow field is symmetric and thus the velocity components normal to the chamber axis fluctuate around zero and their average value is approximately zero.

The dynamic flow regimes in opposed jets mixers is characterized by the sequential formation of vortices. The time evolution of the local velocities is caused by the vortices that pass through the probed points. These vortices have a chaotic behavior due to the complex interactions between consecutive vortices that change in terms of size and shape. The chaotic nature of the vortices formation process yields chaotic time series.

The differences between the flow fields in prismatic and cylindrical chambers are now analyzed from the time evolution of the velocity components at the probed points (Figures 15-17)). This analysis and the flow maps of Figures 12-14 give a characterization of the dynamic evolution of the flow throughout the mixing chamber. The first and most striking observation from the time histories analysis, at all probed points, is the fact that the amplitude of the oscillation of v_x is larger in the prismatic chamber.

In the cylindrical chamber the time histories of v_x show similar features for the impingement point ($y = -5$ mm) and for $y = -11$ mm. Although, at positions further downstream in the mixing chamber, there is a steep decrease in the amplitude of the oscillations. This is clear from the flow fields that are shown in Figure 12, where it is seen that the flow does not have vortices passing for distances larger than 20 mm from the top of the chamber. Although there is also a decrease on the amplitude of the velocity fluctuations towards the outlet in the prismatic chamber, this drop is not as steep as it is in the case of the cylindrical chamber.

The v_y velocity component has the same direction of the chamber axis and of the main flow direction towards the outlet. The time histories of v_y that are shown in Figure 16 reveal that at the impingement point ($y = -5$ mm) the values of v_y are quite distinct between both chambers. While v_y oscillates around 0 at the impingement region in the cylindrical chamber, it oscillates around 0.2m/s for the cylindrical chamber. In the cylindrical chamber the fluid spreads radially creating a stagnation point in the steady flow case, i.e. all velocity components are null. At the dynamic flow regimes the instantaneous values of the velocity components are not null, although those values fluctuate around zero values. For the prismatic chamber the jets bend towards the outlet and impinge at a region downstream of the axis of the injectors. The vortices upstream the jets circulate with a direction set by the high speed jets, which gives the upper vortices an upward flow direction at $y = -5$ mm. Furthermore, the jets in the prismatic chamber split upon impinging each other in the dynamic flow regimes throwing portions of fluid directed to the closed top of the mixing chamber.

The values of v_y for the prismatic chamber are markedly different after $t = 1$ s. From the dynamic visualization of this simulation results it is observed that, when $t = 1$ s, the jets start flapping, i.e. the jets impingement point is oscillating back and forward and when $t = 1$ s the jets also move up and down. This change in the flow dynamics is seen from the values of v_y that are oscillating around 0.8m/s and after 1s they start oscillating at values around 0.2m/s. This change is also seen from the time histories of v_x that have higher oscillation amplitudes after $t = 1$ s, this is due to the fact that the

jets are moving up and down and so the jets will now pass through the point $y = -5\text{mm}$ while previously the jets were only bent towards the outlet.

The fluctuations of v_y at $y=-11\text{ mm}$ are around the value -0.5 m/s for the cylindrical chamber, and sometimes the velocity reaches positive values, indicating an up flow in positive y direction. The vortices that are formed downstream the jets at $y=-11\text{ mm}$ evolve through the mixing chamber axis, these vortices recirculate fluid to upstream positions in the mixing chamber, which causes the velocity to have positive values in the axial direction. Also of interest is the fact that the values of v_y at $y=-11\text{ mm}$ are around -0.5m/s a value that is approximately the same value of v_y at the steady state, see the time history in Figure 16.

The map of the velocity magnitude in the x -plane $x = 0$ is shown in Figure 18. The map shows at steady state a concentric distribution of the velocity magnitude, i.e. the flow spreads radially and the deceleration in the normal direction to the injectors' axis has the same rate in all directions. Applying a mass conservation equation to the radial distribution of flow it is obtained a measure of the striation thinning that the jets are submitted to. The flow rate from the jets is $q_{inj} = v_{inj}A_{inj} = v_{inj}\pi d^2/4$, the jets are then spread radially and the original thickness, d , changes according to

$$q_{inj} = vA = v\pi w\sqrt{y^2 + z^2} \quad (8)$$

where v is the local velocity magnitude at a distance $\sqrt{y^2 + z^2}$ from the jets impingement point, and w is the local thickness of fluid laminae. The velocities at 2 and 3mm from the jets impingement point are approximately 1m/s and 0.75m/s, respectively, from Equation 5 the thickness of the strias is around 0.37mm and 0.33mm at the same locations 2 and 3mm. The jet thickness is reduced between 4 and 4.5 times, a value that is corroborated from measurements of the laminae thickness made using the PLIF image of Figure 11.

For the dynamic states the v_y in the cylindrical chamber at $y=-11\text{ mm}$ fluctuates around the value of $v_y = 0.5\text{m/s}$, the same value obtained at the steady state, see the time history in Figure 16. The pancake-like structure formed around the jets impingement point by the fluid being spread radially is flapping by action of the vortices formed around the jets, the deformation of the pancake is clear in the PLIF image of Figure 19 obtained at $Re = 200$. The striation is even more intense than in the steady state case, measurements made in Figure 19 show that the jets are thinned by a factor of five to six times at a distance of 2mm from the impingement point. So the thickening of the jets is also observed in dynamic flow regimes in the cylindrical chamber, in addition to the formation of vortices that engulf the two laminas of fluid.

For the prismatic chamber v_y fluctuates around -1.75 m/s and never reaches positive values at this point. This is due to the fact that the jets bend towards the outlet and keep their high speed. Although at the dynamic flow regimes there is a deceleration of the flow after the impingement in relation to the steady case. In the steady state simulation the velocity was close to -3m/s that is approximately the value of the inlet velocity of the jets (3.33m/s). In the dynamics flow regimes the axial velocity never reaches these values of -3m/s , so the strong channeling towards the outlet and death volumes around the merged jet are eliminated when the flow goes from steady regime to dynamic regime.

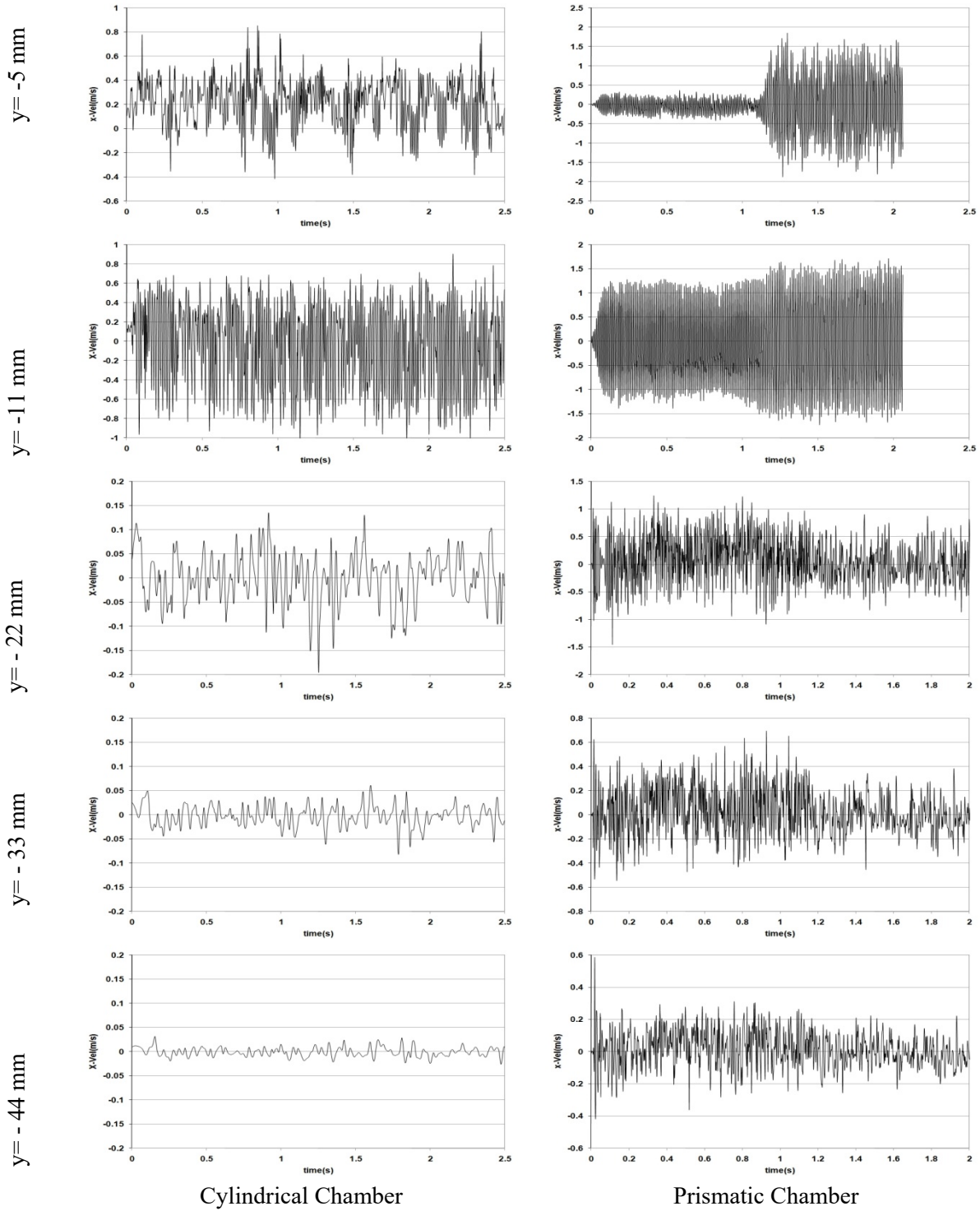


Figure 15. Time histories of v_x

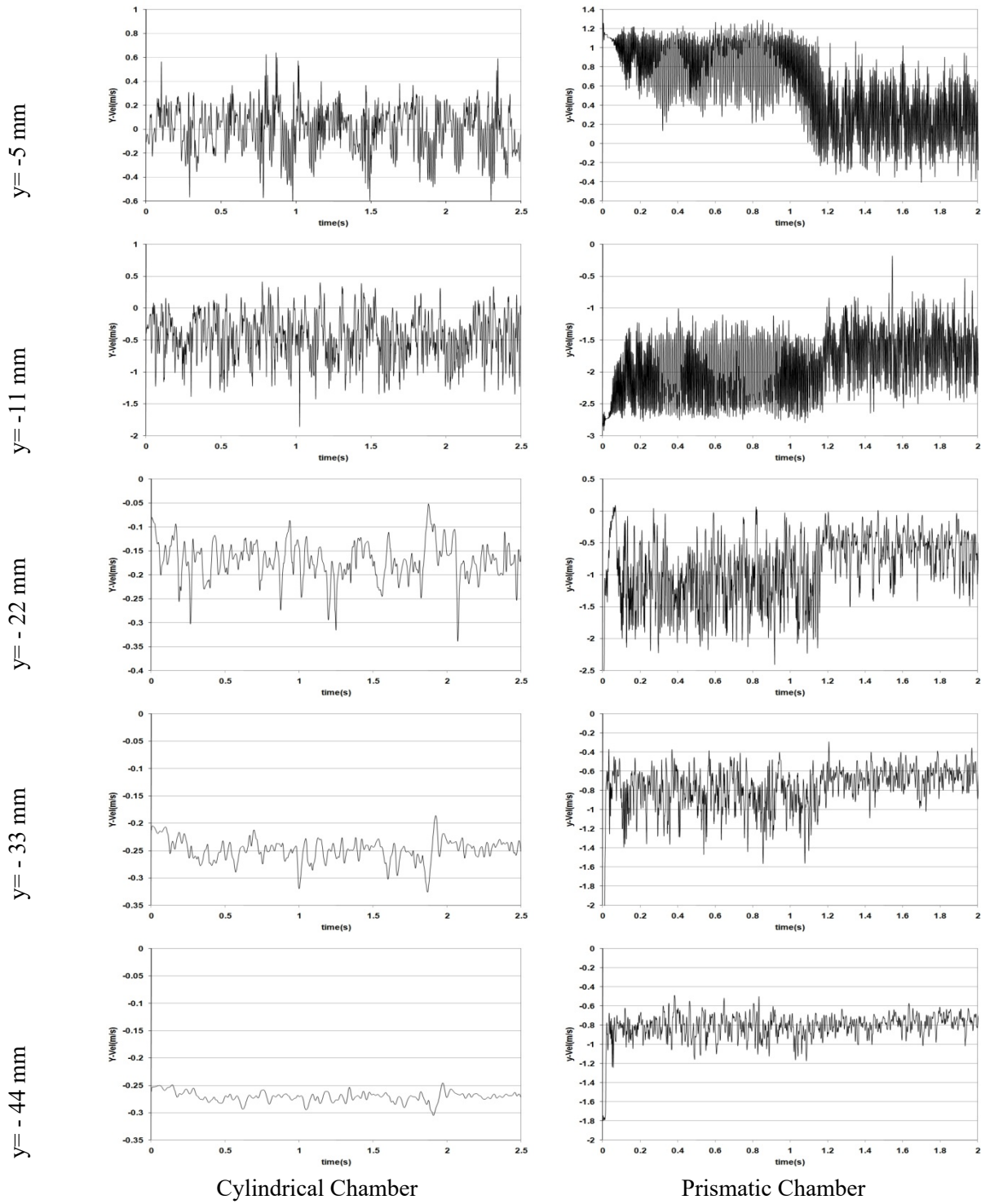


Figure 16. Time histories of v_y

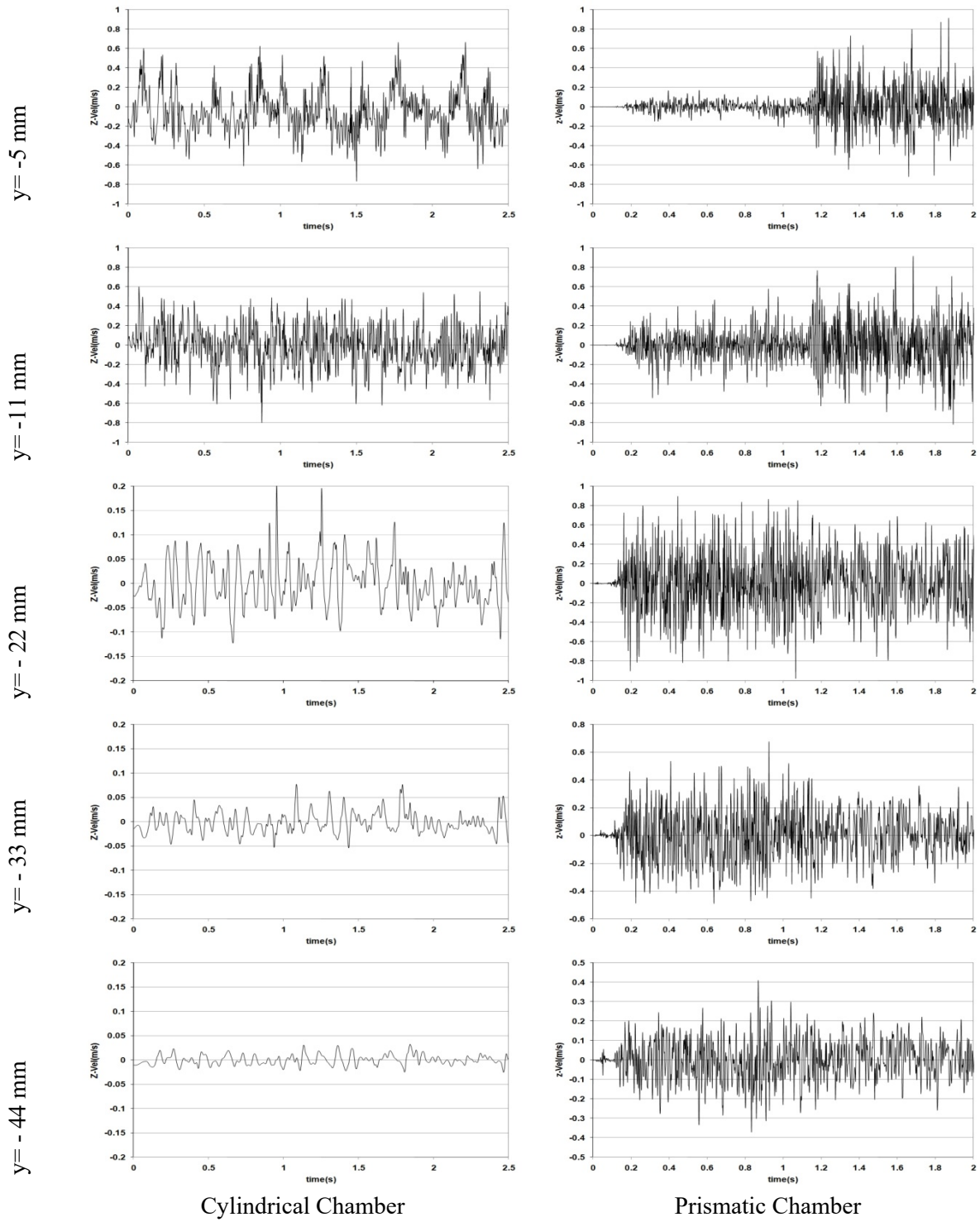


Figure 17. Time histories of v_z

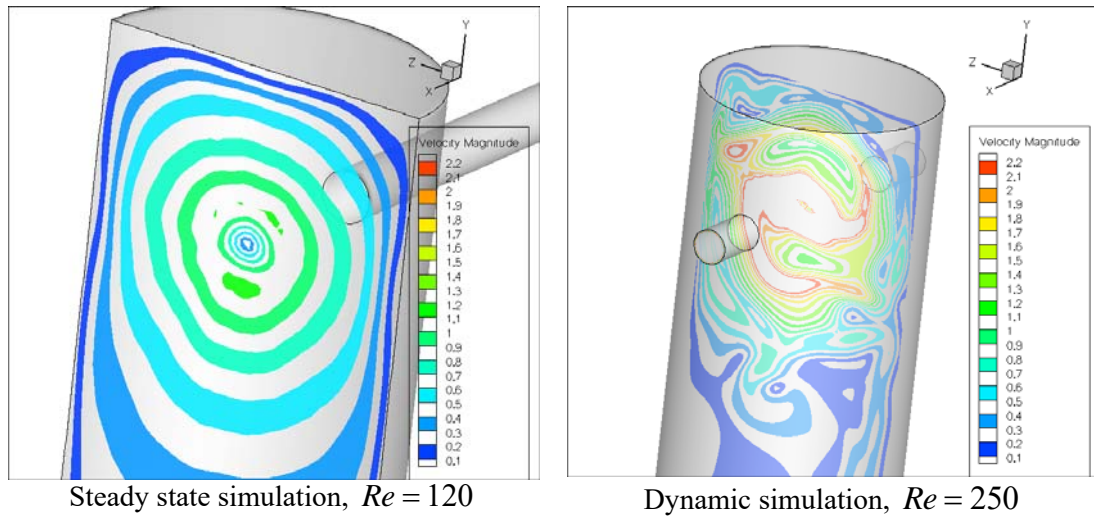


Figure 18. Contours of the velocity magnitude in the plane $x = 0$

After the two upper points, $y = -5\text{mm}$ and $y = -1\text{mm}$, the amplitude of the velocity oscillations decreases, again it's seen a steeper decrease in the cylindrical chamber than in the prismatic one. This is due to the fact that in the prismatic the jets energy is directed towards the outlet without spreading the energy on other directions, while in the case of the cylindrical chamber the jets are spread radially.

The flow inside the prismatic chamber in both x and y directions is mainly governed by the jets: upon entrance in the chambers the jets have a strong velocity in the x direction, and after impinging each other the fluid is forced to move in y direction towards the outlet. However, the only mechanisms leading the flow in z directions are the shear stresses from the wall, there is a gradient v_x and v_y from the chamber walls towards the chamber axis. Although the jets enter through the entire depth of the prismatic chamber the amplitude of the oscillations of v_z at the impingement point and $y = -1\text{mm}$ point, are approximately in the same range in the cylindrical and in the prismatic chamber. Moreover, as the points go down towards the outlet, it is observed that the amplitude of the oscillations are higher inside the prismatic chamber. Although the flow patterns in the prismatic chamber are in general better simulated with the 2D model [4] there is a strong dynamics of the flow in the z direction. Although the strong fluctuations of v_z in the prismatic chamber, the average flow field is markedly 2D. Furthermore, the instantaneous flow maps of the prismatic chamber have many common features with the 2D CFD simulations.

Cylindrical Chamber

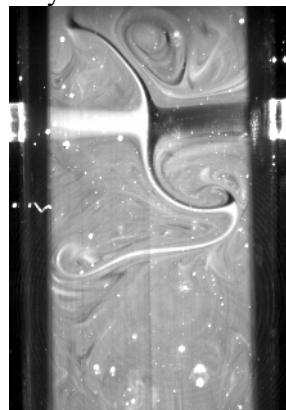


Figure 19. PLIF image of the cylindrical chamber for $Re = 200$

3.2.3. Flow dynamics – frequency analysis

The power spectra of the time histories of the velocity components were calculated to get further insight into the flow dynamics. The power spectra of u_x , u_y and u_z are shown in Figures 20-22, respectively. In the cylindrical chamber, two distinct frequencies are observed from the power spectra of u_x : at the jets impingement point, $y = -5\text{mm}$ there is a low frequency peak in the power spectra at a frequency value below 50Hz; at the $y = -1\text{mm}$ point, the u_x oscillations are in the range of 50 to 100Hz, around 80Hz. At downstream positions of the $y = -1\text{mm}$ point the flow oscillations have frequencies below 50Hz. The higher frequency oscillations were proposed by [26] to be associated with the rate of vortices formation. The lower frequencies are observable from the power spectra and also from the oscillation of u_x in the time histories of Figure 15, however they have not been identified to any of the observed flow mechanisms, so far.

The power spectra of u_x time series in prismatic chamber reveals one typical frequency of oscillation, observable from the energy peak of the power spectra at 86 Hz. For the impingement point down to the point at $y = -22\text{mm}$ the same typical frequency of 86 Hz is observed. The Strouhal number of this frequency is around 0.12, and the Strouhal number is defined,

$$St = \frac{f d}{u_{inj}} \quad (9)$$

where f is the typical oscillation frequency obtained from the power spectra, u_{inj} is the surface velocity at the injectors and d is the width or diameter of the injectors for the cases of prismatic and cylindrical mixing chambers, respectively. The Strouhal number, $St = 0.12$, is very close to the value obtained from 2D simulations, $St \approx 0.1$ ([26] and [27]). The prismatic chamber has only one typical well defined frequency, while the 2D chambers have a second lower frequency, $St \approx 0.03$, at positions downstream in the mixing chamber associated with a vortex street that extend throughout the entire width of the 2D mixing chamber ([26] and [4]). In the prismatic chamber at positions further downstream in the mixing chamber the vortices are replaced by a meandering of the merged jet as can be seen from the vector maps of Figure 12. Because of this the flow oscillation cease to exhibit a clear oscillation and the power spectra have no clear energy peaks downstream the $y = -22\text{mm}$ point.

In the cylindrical chamber, the energy peaks in the power spectra for the u_y and u_z velocity components are at approximately the same frequencies range, 50Hz to 100Hz, than in the u_x power spectra down to the $y = -1\text{mm}$ point. The jets oscillations are thus markedly 3D and within a range of frequencies, i.e. typical frequencies of oscillation, that are the same for the three velocity components. Downstream in the cylindrical mixing the same low frequency energy peak is observed for the three velocity components.

The oscillation frequencies in the prismatic chamber around the jets impingement point, points $y = -5\text{mm}$ and $y = -1\text{mm}$, have a frequency of oscillation of u_y approximately twice the frequency of oscillation of u_x . Each of the opposed jets pushes the jets impingement point to the opposite side of the mixing chamber, which makes the jets impingement point to move back and forward. When one of the jets starts pushing the impingement point this jet also moves in the y direction towards the top of the mixing chamber; before pushing the jets impingement point completely into the opposite side of the mixing chamber the jet inverts the movement in the y

direction and moves towards the outlet. So, for half oscillation in the y direction the jet has a full oscillation in the x direction. This mechanism is only observable from the dynamic visualization of the velocity contour plots from the CFD simulation.

Although the flow in prismatic chamber have clearly observable oscillations in the z direction, the power spectra of Figure 22 does not show any clear energy peak, or higher energy region, associated to any frequency value or range. The oscillations caused by the evolution of flow structures, such as the vortices downstream the jets impingement point, generally are associated with a typical frequency. The oscillations in the z direction probably are not being governed by a specific flow pattern.

This analysis is one of the first efforts on the analysis of the 3D effects on the flow dynamics in opposed jets mixers. The flow characterization is not as thorough as the characterization of the 2D flow field in opposed jets mixers. The detailed level of characterization of the 2D flow field enabled [26] to associate each typical frequency of the flow to a specific flow feature. In this study some mechanisms for the flow dynamics were already suggested, however only a more thorough characterization of the dynamic flow field will allow to propose mechanisms that explain this dynamics of the flow.

3.2.4. Turbulence models

While the flow field and time series analysis give certain differences of the two chambers studied, they are not enough to characterize mixing and drive conclusions on which of them is a better mixer. Since the aim is to compare the two given geometries in terms of mixing efficiency, one should look at the turbulence characteristics and the shear flow further. The smaller the length scales, then the mixing scale is smaller and hence the rate of mixing at the smallest scale is faster [28]. If homogenous isotropic turbulence is assumed, the smallest characteristic spatial scale is the Kolmogorov scale defined as [29]

$$\lambda_K = \left(\frac{\nu^3}{\epsilon}\right)^{1/4} \quad (10)$$

Where ν is the kinematic viscosity and ϵ is the turbulent energy dissipation rate. Additionally, the turbulent fields, turbulent kinetic energy (the integral of the three dimensional power spectra), and turbulent energy dissipation rates would be helpful to point the differences further. In Fluent™, it is possible to calculate all these parameters numerically. For this purpose, the randomly chosen solutions at different time scales were solved just for turbulence using low Reynolds $k - \epsilon$ method. Since the solutions for turbulence parameters and transport parameters were run for some time instants only, the values will not be compared but a visual insight will be provided.

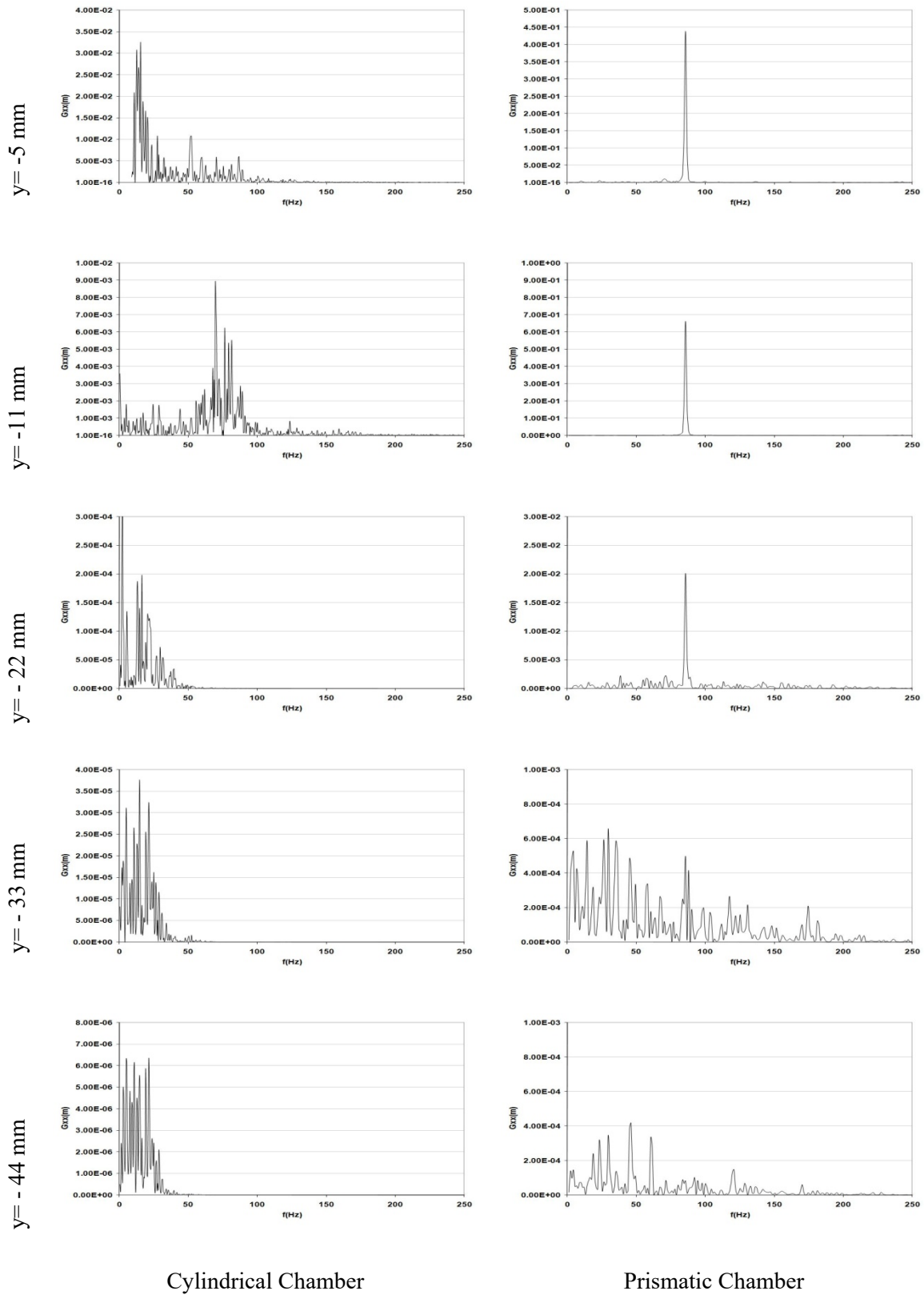


Figure 20. Power Spectra of time histories of v_x

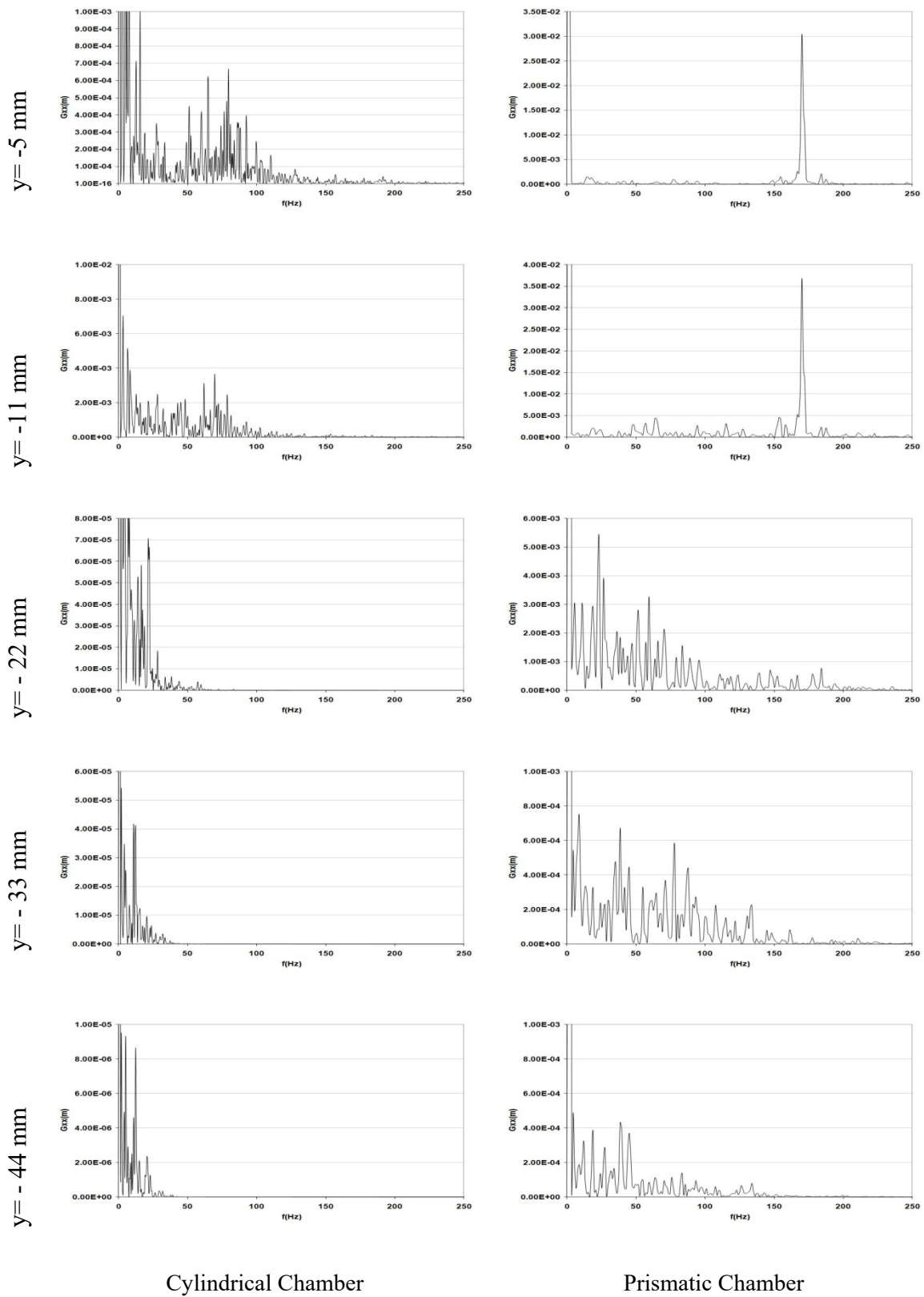
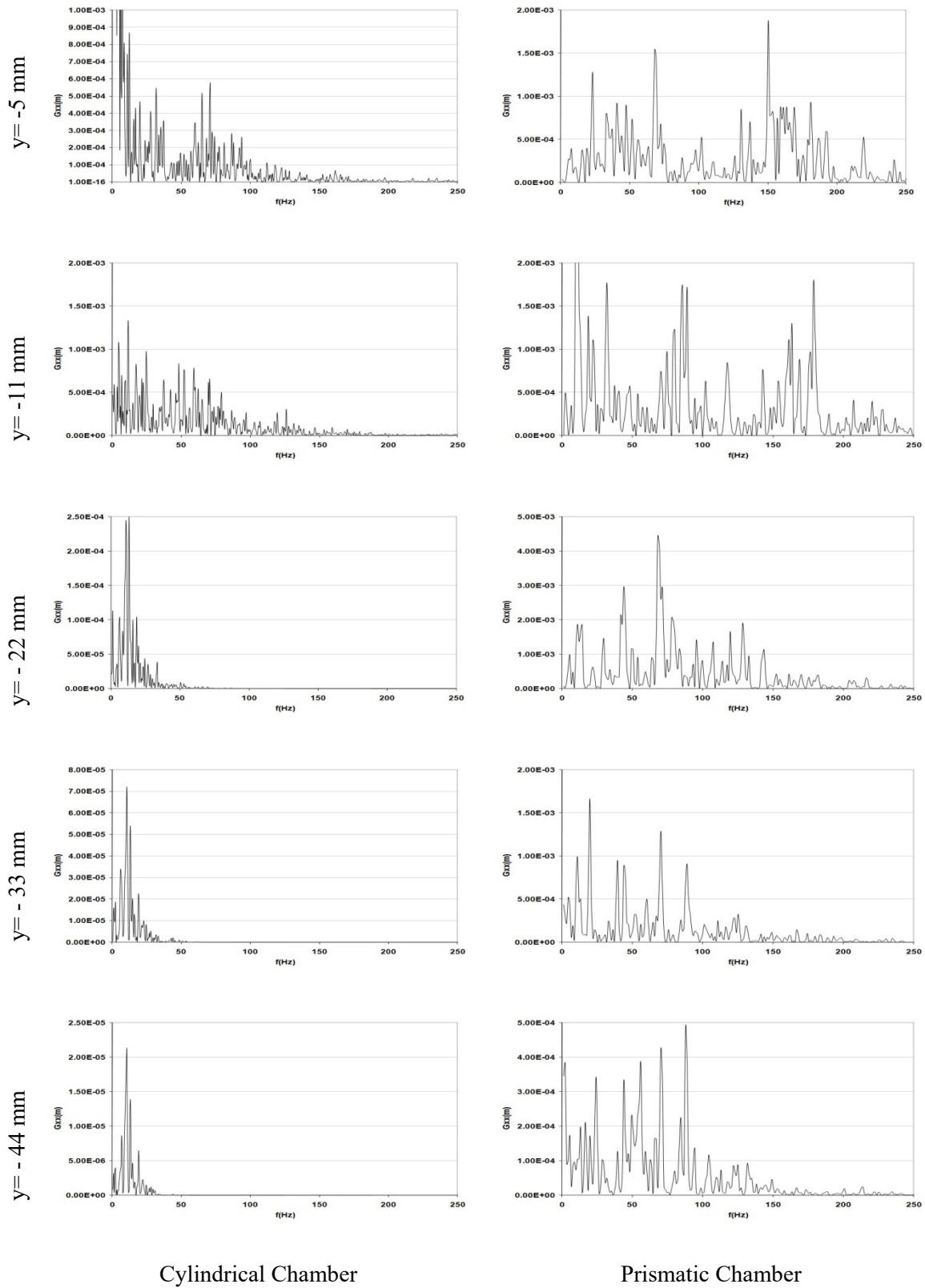


Figure 21. Power Spectra of time histories of U_y



Cylindrical Chamber

Prismatic Chamber

Figure 22. Power Spectra of time histories of U_z

Figure 23 shows the contours of turbulent kinetic energy (TKE) in $z=0$ planes at three different time instants for both the chambers. As the two jets are deflected and/or impinge to each other, they produce higher intensity of fluctuations in velocity, consequently, TKE is higher around the impingement region as expected. In the regions, where the fluctuations of the velocity are smaller the TKE has lower values. As the time histories and power spectra of the velocities suggest, while the cylindrical chamber is active up to 11 mm from the top of the chamber, having higher values of TKE, the prismatic chamber has higher values of TKE until 22 mm down from the top of the chamber as it can also be seen in Figure 23. It is well known that for a conventional cylindrical chamber, the zone of intense mixing is limited to a small volume which is around the impingement point of the complete volume of the chamber [30].

The turbulent region where the shear flow dominates the hydrodynamics can be seen in terms of energy dissipation rate in Figure 24 and by turbulence intensity given in Figure 25. Highest values of the dissipation and turbulence intensity are near the impingement point, and impingement region where the flow is dominated by the fully developed vortices. For the rest of the chambers, since the Reynolds Number is low, turbulence is not sustained for the whole chamber and the dissipation of energy is higher than the production [31].

Another parameter worth to present is the Turbulent Reynolds Number, as it is reported that for the existence of an inertial range a Turbulent Reynolds Number greater than 100 is required [30]. Figure 26 shows the contours of Turbulent Reynolds Number in $z=0$ planes for three different time instants. The turbulent Reynolds Number is in the range of 600 around the impingement region however the higher values of Turbulent Reynolds Number take an oval shape in contour plots, whereas the prismatic chamber provides a rectangular region longer in $-y$ direction. While the Turbulent Reynolds Number value drops down dramatically below the active impingement region in cylindrical chamber, it drops down gradually in prismatic chamber. Apparently, from the results of the recorded velocity data and turbulence parameters, the region where the strong vortex dynamics occurs is larger inside the prismatic chamber.

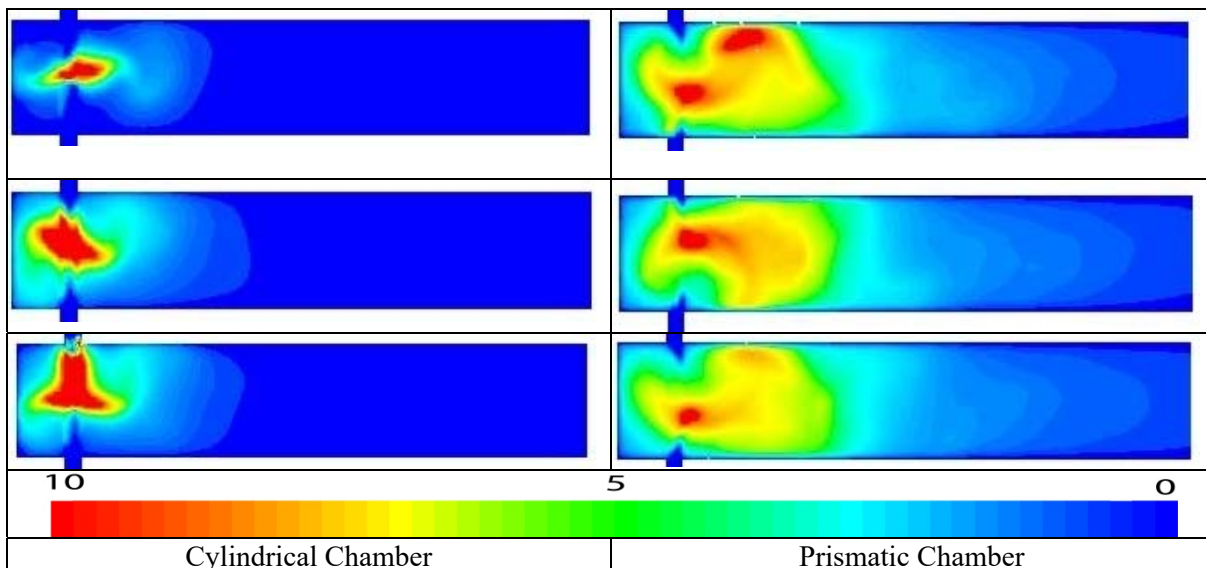


Figure 23. Instantaneous Contours of Turbulent Kinetic Energy (m^2/s^2) in $Z=0$ planes

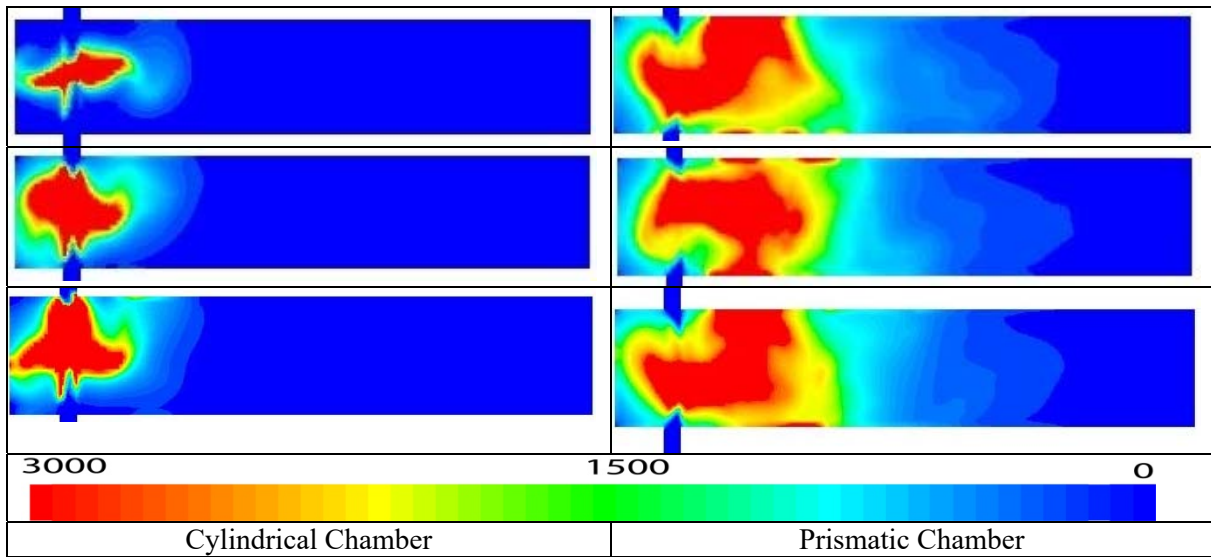


Figure 24. Instantaneous Contours of Turbulent Dissipation Rate (m^2/s^3) in $Z=0$ planes

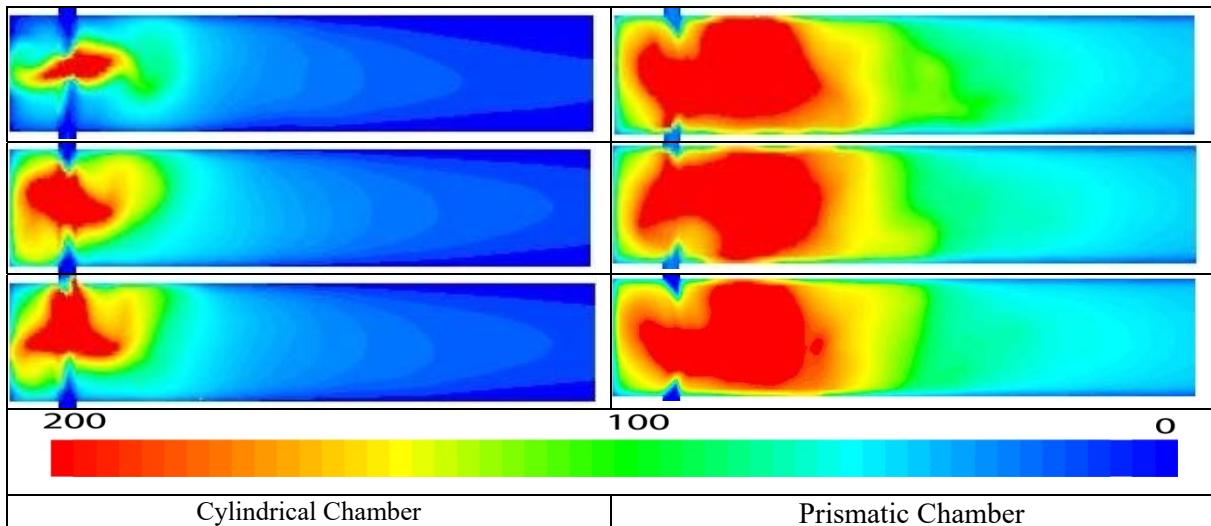


Figure 25. Instantaneous Contours of Turbulence Intensity (%) in $z=0$ planes

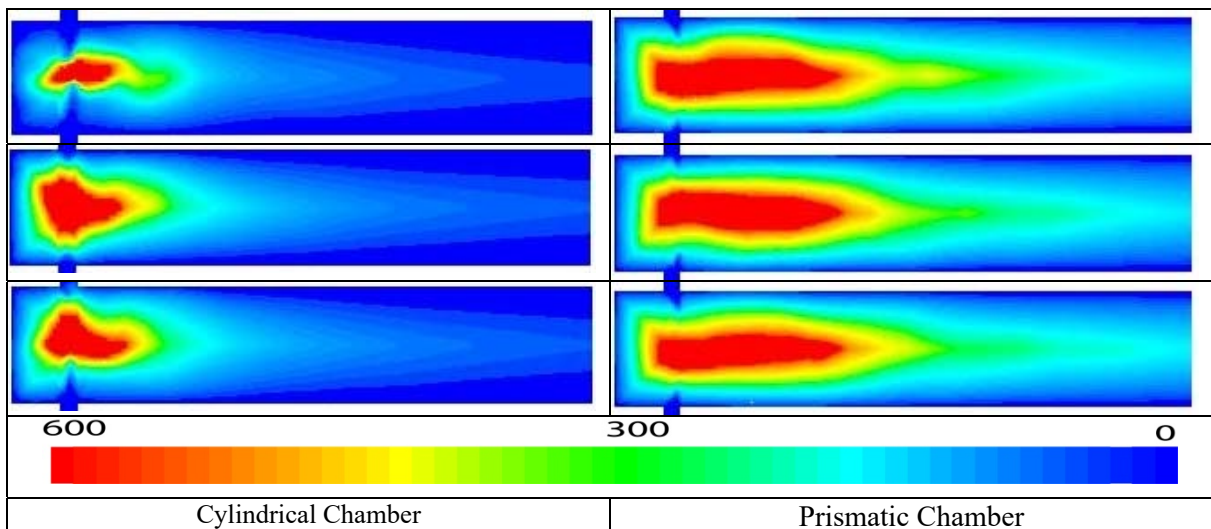


Figure 26. Instantaneous Contours of Turbulent Reynolds Number in $z=0$ planes

3.2.5. Mixing simulations

As the last step to compare the geometries mixing performance is evaluated from tracer simulation and measurement of the fluid homogeneity inside the chamber. The same procedure is being followed however this time randomly chosen dynamic solutions available are solved only for mass transport equations. These values are belonging to some of the time instants, which may fall on the average values or somewhere in the fluctuating values. For this reason, instead of numerical comparison, a visual comparison in some random time instants is provided. Nevertheless, they provide useful information to compare the geometries. A constant diffusivity of $D_m = 2.88 * 10^{-6} \text{ m}^2\text{s}^{-1}$ was used for both of the chambers giving a Schmidt Number of $Sc = 5.79$. Two equal species A and B, having equal physical properties are fed into the mixing chambers and the contours of the mass fraction of A are shown for several time instants.

Figure 27 shows the contours of mass fraction of A for seven randomly chosen time instants at $z=0$ planes. The difference is very obvious between the mixing performances of the two different geometries. Prismatic chamber offers poor mixing efficiency with respect to the cylindrical chamber with the given configurations. For the prismatic chamber, although the fluid stretching and oscillations are clear in the plots, the segregation patterns are easily seen, a significant part of the liquid leaves the chamber without mixing efficiently in the axial centre plane of the chamber. On the other hand, in the cylindrical chamber, it is seen that mixing is more intense and sudden, the green colour indicating a homogenous distribution is dominant immediately below and above the impingement point. To see the distributions in other planes, for a chosen time instant, the distribution in y, z and x planes are presented in Figures 28-30 respectively. It can be seen from Figure 28 that as the jets impinge to each other in the cylindrical chamber, they stretch and bend in z direction, which makes the boundary layer thinner between the two fluids and start to mix right there. As most of the transfer is complete in the impingement point in $y=0$ plane, the planes below have better homogeneity with respect to the planes in prismatic chamber. In the prismatic chamber, as the jets impinge, they move up and down, i.e., move in y direction. Although they also move in x direction, because there is less movement in z directions, there is no mechanism to make the boundary layer thin enough and mixing do not take place in the impingement plane of $y=0$ but just the diffusion of species. So, the mixing starts to take place under the impingement plane and the segregated clusters of fluids can be seen easily in all the y planes.

For all the z planes shown in Figure 29, it can be seen that the distribution of the species are more homogenous for the cylindrical chamber. While the flow patterns in the planes differ in prismatic chamber, the flow patterns of the jets are the same in all the planes as the jets have the same depth with the chamber itself. The flow pattern and hence the distribution of the species do not change significantly in 1 mm, although it differs significantly in 3 mm.

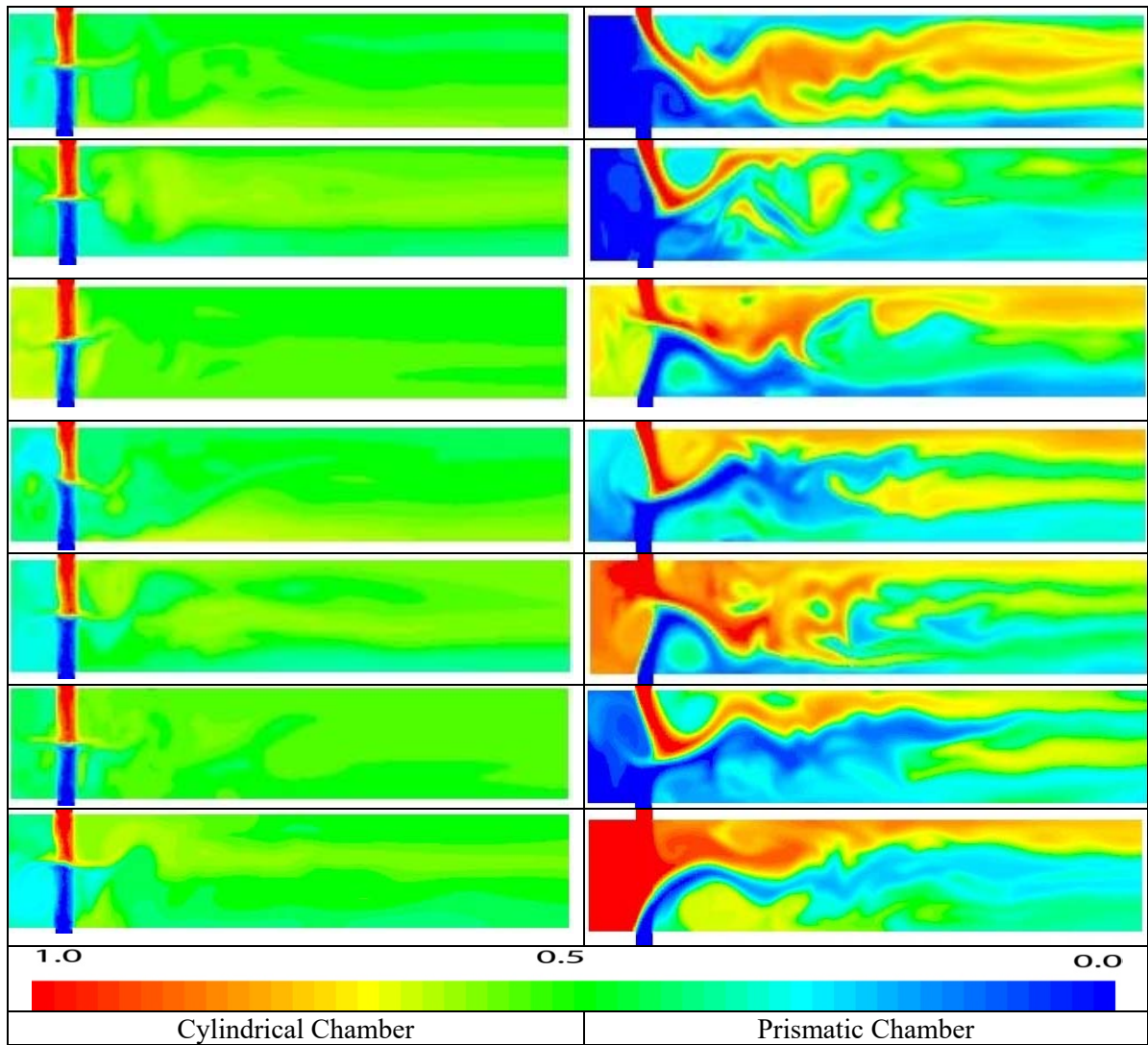


Figure 27. Contours of Mass Fraction of A in $z=0$ planes

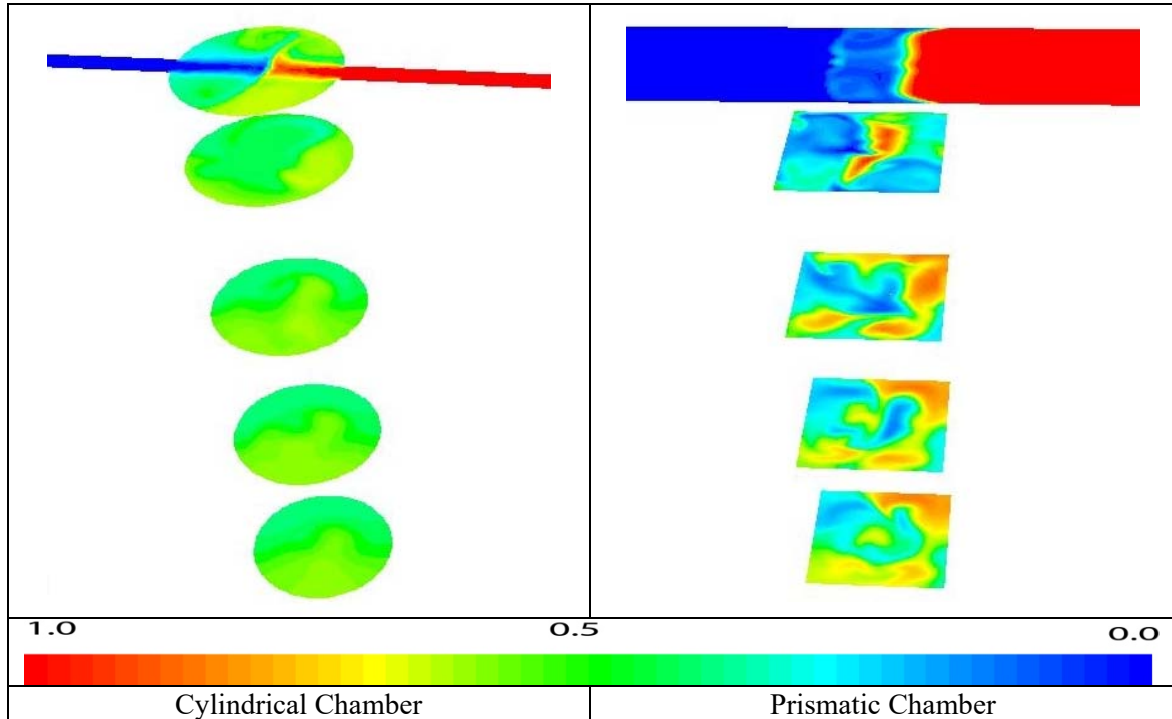


Figure 28. Contours of Mass Fraction of A in y planes for the chosen time instant

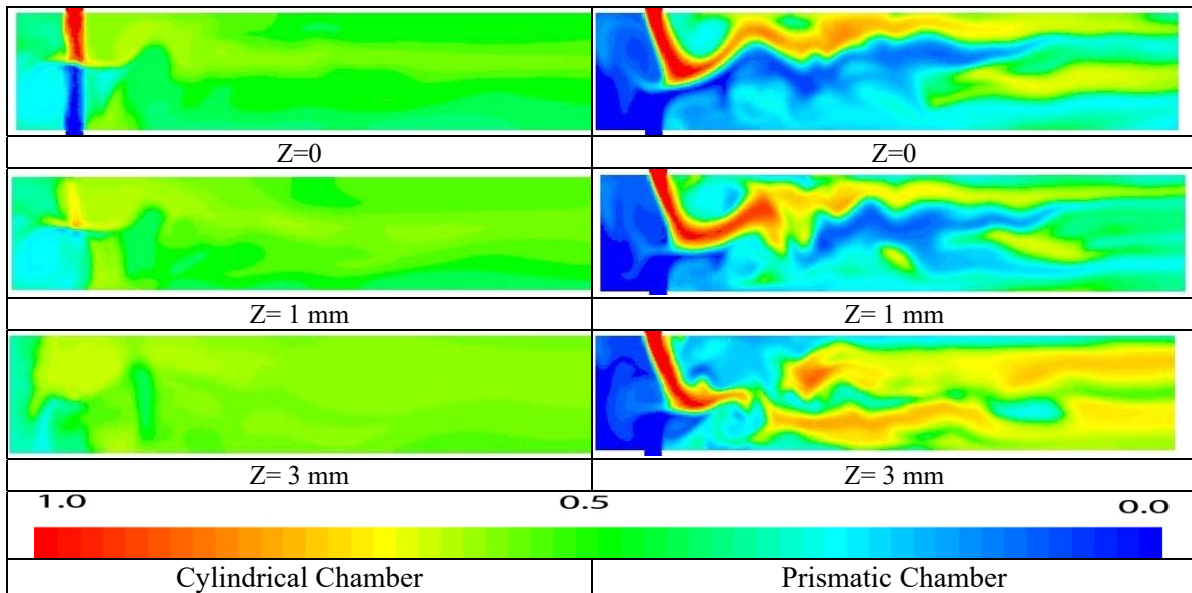


Figure 29. Contours of Mass Fraction of A in z planes for the chosen time instant

The negative effect of having the jets all chamber depth long is also seen in x planes shown in Figure 30. Similar to the other planes, x planes of cylindrical chamber presents more homogenous distributions of the species with respect to the prismatic chamber. It can be seen that the red line in $x=3$ mm plane which indicates the jet feeding the species A, has a higher position in y axis than the ones in $x=1$ mm and $x=0$ planes, with $x=0$ plane being in the lowest position. This shows that the jet feeding the species A is bent downwards as it can be seen from the contours in z planes. The contour plots in x planes show the negative effect of the fluids being on thick laminas and unreachable by the other fluid. While in $x=0$ plane, where the two fluids are in direct contact, the amount of green area is higher, at $x=3$ mm plane, the dominant red color can be seen indicating poor contact of the fluids in that region.

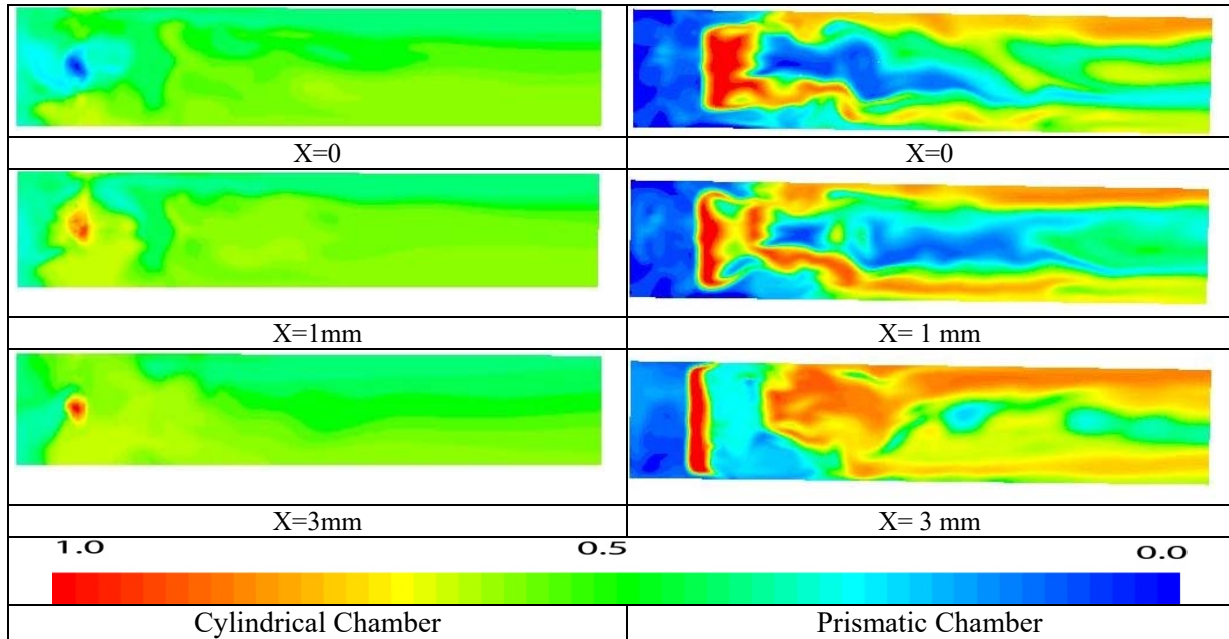


Figure 30. Contours of Mass Fraction of A in x planes for the chosen time instant

While the time series and turbulence fields' analysis showed that the prismatic chamber presents turbulence in greater area, the tracer simulations showed that the mixing efficiency is poorer. While calling the chambers as cylindrical and prismatic, it should be underlined and emphasized again that it's not exactly the geometry of the chamber, but it's the feeding lines what makes the difference in this study. While the cylindrical chamber is fed by 1.5 mm diameter cylindrical jets, the prismatic chamber is fed by jets having rectangular cross section with a side length equal to the depth of the reactor, thereby not giving room for bulk circulation in z directions. While providing higher turbulent values, the absence of circulation in z directions bring couple problems which can be summarized as the following:

- When the jets move in x and y directions in the impingement point, most of the energy is transferred in to the y direction, causing faster velocity in -y direction and hence leaving the reactor segregated.
- When the jets have bigger cross sectional area, 1.5 mm in y direction and 10 mm in z direction, they form a thick boundary layer with less surface area, and as they roll downstream towards the outlet, the diffusion take place only on the interfacial surface between the two streams.

This study shows that the prismatic chamber provides higher turbulence values throughout the flow field, and hence better mixing of fluid A and B would be expected, however, it fails to bring A and B in contact efficiently.

This disadvantage can be overcome by reducing the length of the jets on the z direction, giving enough room for flow circulation. The rule of thumb for this is the fact that the largest scale of segregation must be smaller than the largest scale of motion inside the chamber [32]. To find the optimum side length of the jets can be another subject and probably can be carried out by the observations of [13], made for the impingement distance in x direction.

4. CONCLUSIONS

For both 3D geometries, there is an active region, where the eddies dominate the flow in terms of shear flow, showing turbulence characteristics, and a region where the flow is more dominated by the laminar flow and not very active in terms of mixing. For the cylindrical chamber, the active region is the top region of the chamber around the impingement point, and valid up to about 20 mm down from the top of the chamber.

Although the prismatic chamber is designed 3 dimensionally but in a way to mimic a 2D flow, it shows strongly 3D hydrodynamics because of the complex interactions of vortices with each other. Prismatic chamber of the given configuration produces well defined repeating vortices around the impingement point which move as solid bodies until 22 mm downstream the top of the chamber. Unlike the cylindrical chamber, the power spectra of x and y velocity time series give a well-defined peak at certain frequency values.

Power spectra of x velocities give the same Strouhal number than the 2D chamber, however without spread in energy. [27] has shown that a well-defined peak is not a sign of chaotic mixing alone and can be a sign of oscillatory flow with poor mixing.

For better mixing performance, freedom of movement in all three directions should be provided. Moreover, this freedom of movement should have enough room to make the boundary layer thinner as well as create self-sustained oscillations.

This study shows that on one hand CIJ promotes a more intense striation of the initial flow scales when compared to the T-jets, on the other hand the latter promotes a broader impingement region and allows larger inlet areas, i.e. higher throughputs, for the same initial scale. The choice of the mixer should then be the trade-off between these two factors.

ACKNOWLEDGEMENTS

This study was performed in Laboratory of Separation and Reaction Engineering (LSRE), at the Faculty of Engineering, University of Porto, Portugal. The author acknowledges the friendly and supportive atmosphere of LSRE and the guidance of José Carlos Lopes, Madalena Dias and Ricardo Santos. The author also acknowledges the financial support of FCT with the reference SFRH/BD/18901/2004.

REFERENCES

- [1] Lee LJ, Ottino JM, Ranz WE and Macosko CW. Impingement mixing in reaction injection molding. *Polymer Engineering & Science*, 1980; 20(13): p. 868-874.
- [2] Gradl J, Schwarzer H-C, Schwertfirm F, Manhart M and Peukert W. Precipitation of nanoparticles in a T-mixer: Coupling the particle population dynamics with hydrodynamics through direct numerical simulation. *Chemical Engineering and Processing: Process Intensification*, 2006; 45(10): p. 908-916.
- [3] Johnson BK and Prud'homme RK. Chemical processing and micromixing in confined impinging jets. *AIChE Journal*; 2003. 49(9): p. 2264-2282.
- [4] Santos RJ, Teixeira AM, E. Erkoç MA, Sultan, A. Karpinska M, Dias M and Lopes JCB. Validation of a 2D CFD Model for Hydrodynamics' Studies in CIJ Mixers. *International Journal of Chemical Reactor Engineering*, 2010; 8: p. A32.

- [5] Gillian JM. and Kirwan DJ. Identification and correlation of mixing times in opposed-jet mixers. *Chemical engineering communications*, 2008; 195(12): p. 1553 - 1574.
- [6] Trautmann P. and Piesche M. Experimental investigations on the mixing behaviour of impingement mixers for polyurethane production. *Chemical Engineering & Technology*, 2001; 24(11): p. 1193-1197.
- [7] Jr. JAM. and Lee LJ. Mixing study of L shape mixheads in reaction injection molding. *Journal of Applied Polymer Science*, 1989; 37(8): p. 2295-2312.
- [8] Besbes, S., Mhiri H, Le Palec G, and Bournot, P. Numerical and experimental study of two turbulent opposed plane jets. *Heat and Mass Transfer*, 2003; 39(8): p. 675-686.
- [9] Sultan, MA, Monteiro DS, Dias MM, Lopes JCB and Santos RJ. Influencia de geometria de misturadores em T na dinamica do escoamento, in *Conferencia Nacional em Mechanica de Fluidos, Termodinamika e Energia*. 2009; Bragança.
- [10] Malguarnera SC. and Suh NP. Liquid injection molding I. An investigation of impingement mixing. *Polymer Engineering & Science*, 1977; 17(2): p. 111-115.
- [11] Tucker CL. and Suh NP. Mixing for reaction injection molding. i. impingement mixing of liquids. *Polymer Engineering and Science*, 1980; 20(13): p. 875-886.
- [12] Lee, LJ, Ottino JM, Ranz WE and Macosko CW. Impingement mixing in reaction injection molding. *Polymer Engineering and Science*, 20(13): p. 868-874, 1980.
- [13] Denshchikov VA, Kondrat'ev, VN, Romashov, AN and Chubarov, VM. Auto-oscillations of planar colliding jets. *Izvestiya Akademii Nauk SSSR, Mekhanika Zhidkosti i Gaza*, 1983; 3: p. 148-150.
- [14] Johnson DA, Wood PE and Hrymak AN. The effect of geometrical parameters on the flow field of an opposed jet rim mix head: Equal flow and matched fluids. *The Canadian Journal of Chemical Engineering*, 1996; 74(1): p. 40-48.
- [15] Mahajan AJ and Kirwan DJ. Micromixing effects in a two-impinging-jets precipitator. *AIChE Journal*, 1996; 42(7): p. 1801-1814.
- [16] Sebastian DH and Boukobbal S. Mixhead parameters governing impingement mixing effectiveness for polyurethane reactive injection molding processes. *Polymer Process Engineering*, 1986, 4(1): p. 53-70.
- [17] Jie, Y, Min-quan W, Gan-ce, D and Li, Z. An investigation into impingement jets in cylindrical chamber. *Journal of hydrodynamics*, 1991; p. 90-94.
- [18] Santos R J. Teixeira AM and Lopes JCB. Study of mixing and chemical reaction in rim. *Chemical Engineering Science*, 2005; 60: p. 2381-2398.
- [19] Zhao Y. and Brodkey RS. Particle paths in three-dimensional flow fields as a means of study: opposing jet mixing system. *Powder Technology*, 1998; 100(2-3): p. 161-165.
- [20] Zhao Y. and Brodkey RS. Averaged and time-resolved full-field (three-dimensional), measurements of unsteady opposed jets. *The Canadian Journal of Chemical Engineering*, 1998; 76: p. 536-545.

- [21] Wood P, Hrymak ANR, Yeo Johnson DA and Tyagi A. Experimental and computational studies of the fluid mechanics in an opposed jet mixing head. *Physics of Fluids A*, 1991; 3(5): p. 1362-1368.
- [22] Wong SH, Ward MCL and Wharton CW. Micro T-mixer as a rapid mixing micromixer. *Sensors and Actuators B*, 2004; 100: p. 359-379.
- [23] Nguyen N-T and Wu Z. Micromixers-a review. *Journal of Micromechanics and Microengineering*, 2005; 15(2): p. R1.
- [24] Mansur EA, Ye M, Wang Y and Dai Y. A state-of-the-art review of mixing in microfluidic mixers. *Chinese Journal of Chemical Engineering*, 2008; 16(4): p. 503-516.
- [25] Givi P and Mcmurtry PA. Nonpremixed reaction in homogeneous turbulence: direct numerical simulations. *AIChE Journal*, 1988; 34(6): p. 1039-1042.
- [26] Santos RJ, Erkoç E, Dias MM and Lopes JCB. Dynamic behaviour of the flow field in a rim machine mixing chamber *AIChE Journal*, 2009; 55(6): p. 1338-1351.
- [27] Erkoç E, Santos, RJ, Nunes MI, Dias MM and Lopes JCB. Mixing dynamics control in RIM machines. *Chemical Engineering Science*, 2007; 62(18–20): p. 5276-5281.
- [28] Paul EL, Atiemo-Obeng V and Kresta SM. *Handbook of Industrial Mixing*. Wiley, 2003:
- [29] Tennekes H. and Lumley JL. *A first course in turbulence*. Cambridge Mass.: The MIT Press. 1972.
- [30] Liu Y. and R.O. Fox, CFD. Ppredictions for chemical processing in a confined impinging-jets reactor. *AIChE Journal*; 2006; 52(2): p. 731-744.
- [31] Schwertfirm F, Gradl J, Schwarzer HC, Peukert W and Manhart M. The low reynolds number turbulent flow and mixing in a confined impinging jet reactor. *International Journal of Heat and Fluid Flow*, 2007; 28(6): p. 1429-1442.
- [32] Hansen L, Guilkey JE, McMurtry PA and Klewicki JE. The use of photoactivatable fluorophores in the study of turbulent pipe mixing: effects of inlet geometry. *Measurement Science and Technology*, 2000; 11(9): p. 1235.